Dynamical Climatology

A scheme for predicting layer clouds and their water content in a general circulation model.

by

R.N.B. Smith

DCTN 68

August 1988

Meteorological Office (Met. O. 20)
London Road
Bracknell
Berkshire RG12 2SZ

DYNAMICAL CLIMATOLOGY TECHNICAL NOTE NO. 68

A SCHEME FOR PREDICTING LAYER CLOUDS AND THEIR WATER CONTENT IN A GENERAL CIRCULATION MODEL.

by

R N B Smith

This paper has been submitted for publication.

Met O 20 (Dynamical
Climatology Branch)
Meteorological Office
London Road
Bracknell
Berkshire, UK RG12 2SZ

Revised June 1989

Note: This paper has not been published. Permission to quote from it should be obtained from the Assistant Director of the above Meteorological Office branch.

Summary

A cloud water variable has been included in the Meteorological Office atmospheric general circulation model. The cloud amount and water content are generated by a scheme which assumes a distribution of thermodynamic and water content variables about their grid-box mean values. A parametrization of the rate of depletion of cloud water by precipitation is included. The model's boundary layer mixing is reformulated in terms of variables conserved during changes of state of water, allowing a more realistic calculation of atmospheric stability in cloudy regions.

The scheme produces realistic cloud distributions and the predicted cloud water content verifies well against microwave radiometer data in all regions except the mid-latitudes of the summer hemisphere. The parametrization of cloud optical properties in terms of the cloud water content will be an important future development of the model.

1. Introduction

Until recently the treatment of clouds in large scale numerical models of the atmosphere has lacked the complexity required to represent the processes which cloud physicists have identified as important. The first Atmospheric General Circulation Models (AGCMs) and Numerical Weather Prediction (NWP) models did no more than specify the cloud amounts and radiative properties for the radiation calculations using estimated climatological values. When AGCMs are used for climate simulation and perturbation experiments this non-interactive approach to the radiative effects of clouds has the disadvantage of eliminating almost all cloud-radiation feedbacks from the model. For weather prediction longer-term feedbacks are not so important. However, the ability to forecast surface temperatures, fog and other sensitive weather elements is degraded by using radiative fluxes based on cloud unaffected by the predicted synoptic and smaller scale features.

In order to overcome these deficiencies most models now include schemes to calculate cloud amounts interactively from model variables such as relative humidity and convective activity. Such schemes vary in complexity and detail. The U.K. Meteorological Office AGCM, in its current standard form (Slingo et al., 1988), calculates layer cloud amounts as a simple function of relative humidity and convective cloud amount from the amount of water condensed in any moist convection. In the ECMWF model cloud amounts also depend on quantities such as vertical velocity and lapse rate (Slingo, 1987). These diagnostic methods for cloud prediction are easy to implement and, as shown by Slingo (1987), can produce realistic simulations. However, they are purely empirical and have little basis in cloud thermodynamics and microphysics. To introduce this physics, at least the cloud water content is needed.

The radiative properties of clouds depend on their water content, the phase of the water and the distribution of water droplet or ice particle sizes. These quantities have not been available to large scale modellers and so cloud radiative properties have been specified. The need for interactive radiative properties in climate models has been suggested by those investigating climate change induced by increased atmospheric carbon dioxide and other greenhouse gas concentrations. Somerville and Remer (1984) have suggested that the greenhouse warming may be overestimated in

models with fixed cloud optical properties. Their hypothesis is that a warmer atmosphere leads to increased cloud water contents even if there is little change in cloud cover or height. This implies optically thicker and so more reflective cloud, tending to cool the surface and atmosphere and providing a negative feedback on the perturbed system. Somerville and Remer's conclusion rests on an assumed dependence of cloud water content on temperature which they deduced from the data of Feigelson (1978) and on the realism of their simple radiative-convective model. They did not include the increased longwave emission from radiatively thicker cloud in this model. This is unimportant for low and medium level clouds which have emissivities of almost unity but could be an important effect for cirrus cloud. Somerville and Iacobellis (1987) have included the change in longwave emissivity of cirrus cloud with higher ice water content. Somerville and co-workers admit that their results are merely exploratory and suggestive. Clearly there is a need for those working with AGCMs to continue the exploration. Roeckner et al. (1987) have made an important start on this (although their interpretation of their results has been shown to be erroroneous by Schlesinger (1988)). The first step in this direction is to parametrize or alternatively predict cloud water content. This then has to be combined with parametrized dependences of radiative properties on cloud water.

A further advantage of introducing cloud water into a model is the scope it provides for linking the model's hydrological cycle, moist thermodynamics and cloud prediction. In most current models the latent heating and precipitation associated with layer cloud only occur when the grid-box mean relative humidity reaches saturation even though partial cloud cover may be assumed for radiation calculations at lower relative humidities.

Cloud water can be introduced into a model in two ways: it can be parametrized in terms of other model variables or it can be an explicit prognostic variable of the model. Examples of the former approach are described by Geleyn (1981) and Hense and Heise (1984). Geleyn relates the cloud water content to the saturated specific humidity. Hense and Heise use a more complex, but more physically justifiable, parametrization originally proposed by Sasamori (1975). Sasamori's scheme employs a statistical cloud model and uses the vertical velocity as well as the

relative humidity and temperature to diagnose cloud amount and water content.

The use of an explicitly predicted cloud water content for layer cloud in large scale models was pioneered by Sundqvist (1978) who experimentally included his scheme in the ECMWF global medium range NWP model (Sundqvist, 1981). Roeckner and Schlese (1985) included cloud water in the University of Hamburg AGCM and Roeckner et al. (1987) used this model, with interactive cloud radiative properties, in a climate perturbation experiment to estimate the cloud feedback. Le Treut (1985) has also included cloud water in the Laboratoire de Météorologie Dynamique AGCM.

This paper describes a scheme for predicting layer cloud amount and water content in the Meteorological Office 11-layer AGCM (Slingo, 1985). The cloud water content is a prognostic variable of the model but, in the current version, it is not advected. The treatment of the source/sink of cloud water due to condensation/evaporation is complicated by the desirability of allowing partial cloudiness. We use a statistical cloud model, based on that of Sommeria and Deardorff (1977), in which the cloud fraction and water content are consistently calculated assuming that the variables conserved during phase changes are distributed in a certain way about their grid-box means. The vertical turbulent transport of cloud water and other quantities is treated by formulating the model's turbulent mixing parametrization in terms of the same cloud-conserved variables. The sink of cloud liquid water due to precipitation is parametrized similarly to Sundqvist (1981) but frozen water is assumed to start precipitating with a specified fall speed as soon as it forms.

A parametrization of cloud radiative properties has not been included in the work described here. This, for the reasons given above, will be an important area of future study. It is nevertheless useful to use the model with prescribed radiative properties to assess the scheme's simulation of cloud amount and water content and its impact on other aspects of the model. There is little widespread accurate observational data to validate modelled cloud water contents. However, microwave radiometer measurements of vertically integrated cloud liquid water over oceans are available and are used for verification.

2. The Cloud Water Scheme

a. Cloud water content and its prognostic equation

The scheme introduces an additional prognostic variable representing layer cloud water content (q_c). Strictly, there are two components of this: the specific liquid water content (q_L) and the specific ice content (q_F). This distinction is made on the basis of temperature in the parametrization of precipitation formation described later. (The radiative properties of liquid and ice cloud also differ but a parametrization of these has not been included in the work presented here.) For the general form of the prognostic equation for cloud water the distinction is unecessary; indeed only one extra variable, q_c, is carried in the model. The evolution of q_c is described by:

$$\frac{dq_c}{dt} = (\dot{q}_c)_A + (\dot{q}_c)_D + (\dot{q}_c)_{TM} + (\dot{q}_c)_S + (\dot{q}_c)_P + (\dot{q}_c)_{CV} \qquad (2.1)$$

All the possible sources and sinks of cloud water are represented on the r.h.s. of (2.1). Subscript A denotes the rate of change due to advection; D, horizontal diffusion; TM, vertical turbulent mixing; S, stratiform cloud formation or dissipation (i.e. condensation of water vapour or evaporation of cloud water); P, formation of large scale precipitation and CV, convection.

The advection of cloud water would present problems because numerical advection schemes do not treat well quantities with sharp gradients which have to be kept non-negative - precisely the characteristics of cloud water content. The omission of cloud water advection was found by Roeckner and Schlese (1985) to make little difference in their low-resolution model. However, this may not be true in higher resolution models where advective timescales are shorter and more comparable to those of the other processes. In the work described here cloud water advection, $(\dot{q}_c)_A$, has been omitted as has the horizontal diffusion, $(\dot{q}_c)_D$, normally included with it in models for numerical stability. A possible way of avoiding these numerical problems by advecting cloud-conserved variables will be mentioned later.

No change has been made to the model's convection scheme. Thus there is no <u>direct</u> effect of convection on the large scale cloud water in the model (i.e. the scheme does not include the $(\dot{q}_c)_{CV}$ term in (2.1)). The detrained

convective cloud water is evaporated and added to the environmental humidity field by the convection scheme. The stratiform cloud scheme may then recondense this and so the effect of convection on q_c will come indirectly through the $(\dot{q}_c)_s$ term in (2.1). It would obviously be neater to provide a direct input to q_c from the convection scheme and this is being considered for future versions of the model. However no physical inconsistency or error is introduced by the current procedure.

For completeness and future reference the prognostic equations for specific humidity (q) and temperature (T) are written in the same general form as (2.1):

$$\frac{dq}{dt} = (\dot{q})_A + (\dot{q})_D + (\dot{q})_{TM} + (\dot{q})_S + (\dot{q})_E + (\dot{q})_{CV} \qquad (2.2)$$

$$\frac{dT}{dt} = (\dot{T})_A + (\dot{T})_D + (\dot{T})_H + (\dot{T})_R + (\dot{T})_{TM} + (\dot{T})_S + (\dot{T})_E + (\dot{T})_{MF} + (\dot{T})_{CV} \qquad (2.3)$$

The advection (A), diffusion (D), adiabatic heating (H), radiation (R) and convection (CV) terms are treated exactly as in the standard version of the model. Subscripts TM and S have the same meaning as in (2.1). The subscript E denotes the rate of change due to evaporation or sublimation of precipitation and MF that due to melting or freezing of precipitation. Note that the formation of precipitation does not effect either q or T.

The methods of treating the vertical turbulent mixing (TM), stratiform cloud formation or dissipation (S) and precipitation (P, E and MF) terms in the prognostic equations (2.1)-(2.3) are now described in turn.

b. Turbulent mixing in cloudy regions

The UKMO AGCM has hitherto used a dry turbulence scheme of the first order closure type: that is the turbulent fluxes are calculated from local gradients and stability-dependent transport coefficients. This type of scheme has been retained but it has been modified to allow for cloudy and clear regions. The main feature of the modification is the use of cloud-conserved thermodynamic and water content variables in the manner described by Yamada and Mellor (1979) and Mellor and Yamada (1982). A dry scheme will interpret a temperature lapse rate less than the dry adiabatic value,

as will occur if clouds are present, as statically stable. Mixing between layers in the presence of cloud would therefore be inhibited in the model whereas in reality the latent heating associated with the changes of state of water can increase mixing. An appropriate definition of stability is therefore essential for treating cloudy boundary layer mixing.

We can define thermodynamic and water content variables which are conserved during changes of state of cloud water ("cloud-conserved variables"):

the liquid-frozen water temperature

$$T_L = T - \frac{L_C}{c_p} q_L - \frac{(L_C+L_F)}{c_p} q_F \qquad (2.4)$$

and the total water content

$$q_\omega = q + q_L + q_F = q + q_C \qquad (2.5)$$

where L_C is the latent heat of condensation and L_F the latent heat of fusion. L will be used henceforth to represent L_C or L_C+L_F whichever is appropriate for the state of the cloud water.

Prognostic equations for T_L and q_ω can be derived by combining equations (2.1)-(2.5). They include terms for all the processes involved in changing T, q and q_C except stratiform cloud formation or dissipation (subscript S terms). These terms cancel because T_L and q_ω have been defined so as to be conserved during this process.

The vertical turbulent mixing in the equations for the cloud-conserved variables is represented by flux divergence terms:

$$(\dot{T}_L)_{TM} = -\frac{1}{\rho}\frac{\partial}{\partial z}(\rho\overline{w' T_L'}) \qquad (2.6)$$

$$(\dot{q}_\omega)_{TM} = -\frac{1}{\rho}\frac{\partial}{\partial z}(\rho\overline{w' q_\omega'}) \qquad (2.7)$$

where ρ is the density and z the height. Similar terms also occur in the momentum equations. The prime denotes a turbulent fluctuation from the

mean and the overbar indicates a mean value. Formulating the turbulence effects using the cloud-conserved thermodynamic and water content variables automatically includes the effects of cloud water phase changes on the turbulence (Yamada and Mellor, 1979).

The vertical turbulent fluxes of T_L, q_w and horizontal velocity **u** above the surface are parametrized as

$$\overline{w' T_L'} = - K_H \left(\frac{\partial T_L}{\partial z} + \frac{g}{c_p} \right)$$

$$\overline{w' q_w'} = - K_H \frac{\partial q_w}{\partial z} \qquad (2.8)$$

$$\overline{w' \mathbf{u}'} = - K_M \frac{\partial \mathbf{u}}{\partial z}$$

for the model layer interfaces potentially in, or at the top of, the planetary boundary layer (i.e. at σ = 0.975, 0.900 and 0.790). The fluxes are assumed zero for $\sigma < 0.79$. The turbulent transport coefficients are given by

$$K_{H,M} = \ell^2 f_{H,M}(\widetilde{Ri}) \left| \frac{\partial \mathbf{u}}{\partial z} \right| \quad . \qquad (2.9)$$

The functions of stability f_H and f_M are empirically specified and given in Appendix A. ℓ is a neutral mixing length given by the Blackadar formula

$$\ell = \frac{kz}{1+kz/\lambda} \qquad (2.10)$$

where k=0.4 is the von Karman constant and λ an asymptotic neutral mixing length proportional to the boundary layer depth.

The modified Richardson number, which measures stability, is defined by

$$\widetilde{Ri} \equiv g \left[\tilde{\beta}_T \left(\frac{\partial T_L}{\partial z} + \frac{g}{c_p} \right) + \tilde{\beta}_Q \frac{\partial q_w}{\partial z} \right] \Big/ \left| \frac{\partial \mathbf{u}}{\partial z} \right|^2 \quad . \qquad (2.11)$$

The buoyancy parameters $\tilde{\beta}_T$ and $\tilde{\beta}_Q$ are:

$$\tilde{\beta}_T = \beta_T - \alpha_L \beta_c$$
$$\tilde{\beta}_q = \beta_q + \beta_c \qquad (2.12)$$

where

$$\beta_T = \frac{1}{T} \quad , \quad \beta_q = \frac{\delta}{(1+\delta q - q_c)} \quad , \quad \beta_c = Ca_L\left[\frac{L}{c_p}\beta_T - \frac{\beta_q}{(1-\varepsilon)}\right] \qquad (2.13)$$

$$\varepsilon = 0.622 \ , \quad \delta = 1/\varepsilon - 1 = 0.608 \ ,$$

$$\alpha_L = \left.\frac{\partial q_{sat}}{\partial T}\right|_{T=T_L} = \frac{\varepsilon L q_{sat}(T_L, p)}{RT_L^2} \ , \qquad (2.14)$$

$$a_L = 1/(1+L\alpha_L/c_p) \qquad (2.15)$$

and C is the cloud fraction.

The definition of stability given by (2.11) rests on the hypothesis that the vertical flux of cloud water is given by

$$\overline{w' q_c'} = Ca_L(\overline{w' q_w'} - \alpha_L \overline{w' T_L'}) \qquad (2.16)$$

The r.h.s. of (2.16) reduces to zero when there is no cloud, as might be expected, and for complete cloud cover it becomes the expression derived from the relationship between q_c, q_w and T_L in saturated air. Recently Randall (1987) has challenged the validity of this hypothesis for partly cloudy regions. By considering a mass flux model with an updraught containing liquid water but a downdraught which does not, he arrives at a different result. The more usual relationship (2.16) has been used since Randall's work leaves the convective mass flux and the fractional area of the updraught as undetermined parameters. However, in the light of Randall's discussion the relation (2.16) and the stability parameter $\tilde{Ri}$ derived from it should be regarded as a potentially weak part of this modified turbulent mixing scheme.

Note that the stability now depends on gradients of the cloud-conserved variables and, when there is cloud present ($C > 0$), allows for latent heating and cloud water loading effects through the buoyancy parameter β_c. In the special case of a cloud-free region the modified Richardson number

becomes the more familiar "dry" Richardson number and the turbulence scheme reduces to the more usual formulation.

The expression for the Richardson number, (2.11), needs the values of the buoyancy parameters $\tilde{\beta}_T$ and $\tilde{\beta}_Q$ at layer interfaces in the finite difference formulation. The way these are calculated from the values in the layers on either side of the interface is important, particularly when one layer is cloudy and the other clear. The finite difference form of (2.11) and its implications for the scheme's ability to represent cloud top entrainment instability are discussed in Appendix B.

The surface turbulent fluxes are similarly modified:

$$\begin{aligned}
(\overline{w' T_L'})_* &= - c_H |\mathbf{u}_1| (T_{L1} - T_* + (g/c_p) z_1) \\
(\overline{w' q_w'})_* &= - (q_{w1} - q_{SAT}(T_*, p_*))/r \\
(\overline{w' \mathbf{u}'})_* &= - c_D |\mathbf{u}_1| \mathbf{u}_1
\end{aligned} \qquad (2.17)$$

where subscript 1 indicates the bottom model layer and * the surface. c_D and c_H are the stability-dependent surface drag and heat transfer coefficients respectively. r is the total evaporative resistance given by

$$1/r = \varphi/(r_A + r_S)$$

where $r_A = 1/(c_H |\mathbf{u}_1|)$ is the aerodynamic resistance and r_S is the stomatal resistance to evaporation (r_S = 60 s m^{-1} for evaporation from snow-free land points, zero for all other points). φ is a factor depending on the soil moisture content for evaporation from snow-free land points but set to 1 otherwise. Rogers et al. (1985) have used the parametrization of the surface fluxes given by (2.17) for sea points in a numerical study of the JASIN atmospheric boundary layer. The modified bulk Richardson number which measures the stability of the bottom model layer is given by:

$$\widetilde{Ri}_B = g z_1 [\tilde{\beta}_{T1} (T_{L1} - T_* + (g/c_p) z_1) + \tilde{\beta}_{Q1} r_A (q_{w1} - q_{SAT}(T_*, p_*))/r] / |\mathbf{u}_1|^2 \qquad (2.18)$$

Equations (2.17) and (2.18) take account of the effect on the surface fluxes of any cloud and latent heating in the bottom model layer. As with the parametrizations of the fluxes and Richardson numbers for the layer interfaces above the surface, when cloud amounts and water contents are zero, (2.17) and (2.18) reduce to the "dry" formulation formerly used in the model.

After calculating the turbulent flux divergences of T_L and q_w and incrementing these variables in (2.6) and (2.7), the new values of q_c, q and T are derived using the layer cloud scheme described below.

c. The scheme for forming or dissipating layer cloud

The formulation of the AGCM used before incorporation of the cloud water scheme allowed condensation only when grid-scale supersaturation was reached and then converted the excess water vapour directly to precipitation. With the new cloud scheme condensation can occur before grid-scale supersaturation and the vapour is condensed to cloud water. Also, the conversion from vapour to liquid or frozen cloud water is reversible.

Before describing the details of the cloud scheme an outline of how it is used in the model is presented. In some ways this resembles the way the old scheme for large-scale precipitation was used, which can be represented:

$$\left\{\begin{matrix} T \\ q \end{matrix}\right\} \xrightarrow[\text{over model timestep}]{\text{Processes operating}} \left\{\begin{matrix} T^* \\ q^* \end{matrix}\right\} \xrightarrow[\text{supersaturation}]{\text{Removal of any}} \left\{\begin{matrix} T^+ = fn(T^*, q^*) \\ q^+ = fn(T^*, q^*) \\ ppn = q^* - q^+ \end{matrix}\right.$$

The adjustment back to saturation uses the variables as incremented by the other processes represented in the model (superscript * values). Although this adjustment changes prognostic variables it is diagnostic in the sense that no timestep is involved in the functions giving T^+ and q^+. Note that the step to remove supersaturation could be applied after each process (as long as the precipitation were accumulated) but to save computing time it is done only once each timestep.

The new cloud scheme is used in two similar ways which can be represented:

$$\begin{Bmatrix} T \\ q \\ q_c \end{Bmatrix} \xrightarrow{\text{Process(es)}} \begin{Bmatrix} T^* \\ q^* \\ q_c^* \end{Bmatrix} \xrightarrow[\text{using (2.4-5)}]{\text{Calculations}} \begin{Bmatrix} T_L^* \\ q_w^* \end{Bmatrix} \xrightarrow[\text{Scheme}]{\text{Cloud}} \begin{Bmatrix} T^+ = T_L^* + (L/c_p) q_c^+ \\ q^+ = q_T^* - q_c^+ \\ q_c^+ = q_c(T_L^*, q_w^*) \\ C^+ = C(T_L^*, q_w^*) \end{Bmatrix}$$

or

$$\begin{Bmatrix} T \\ q \\ q_c \end{Bmatrix} \xrightarrow[\text{using (2.4-5)}]{\text{Calculations}} \begin{Bmatrix} T_L \\ q_w \end{Bmatrix} \xrightarrow{\text{Process(es)}} \begin{Bmatrix} T_L^* \\ q_w^* \end{Bmatrix} \xrightarrow[\text{Scheme}]{\text{Cloud}} \begin{Bmatrix} T^+ \\ q^+ \\ q_c^+ \\ C^+ \end{Bmatrix} \quad \text{as above}$$

The functions giving C^+ and q_c^+ are derived below and given in Appendix C.

The second version of the above diagram is appropriate for those model processes which increment the cloud-conserved variables directly, such as the turbulent mixing scheme for the boundary layer described above. The advection scheme could also be used to increment T_L and q_w directly which would effectively advect cloud water without introducing the possible problems discussed in section 2.a. The U.K. Meteorological Office mesoscale model (Golding, 1987) advects cloud-conserved variables but this has yet to be tried in the AGCM.

The cloud scheme operates diagnostically in the same sense as the old large-scale precipitation scheme - no timestep is involved in the calculations. It requires the values of the cloud-conserved variables after they have been incremented using the prognostic equations for the other model processes (i.e. superscript * values). Though the cloud scheme does not change the values of the cloud-conserved variables, T, q and q_c are changed if there is any condensation or evaporation. Like the old large-scale precipitation scheme, the cloud scheme could be applied after every model process, but this is not necessary. However, after any process which increments the cloud-conserved variables directly, it is necessary to use it in order to obtain the new values of T, q and q_c. The rest of this section describes how q_c^+ and C^+ in the above diagrams are obtained from the cloud-conserved quantities.

The calculation of cloud amount and cloud water content uses the cloud distribution concepts developed by Sommeria and Deardorff (1977) and Mellor

(1977). A statistical distribution of the cloud-conserved variables about their grid-box mean is assumed. In the mean the amount of cloud and its water content must clearly depend on the difference between the specific total water content and the saturation specific humidity. The grid-box mean of this quantity in terms of conserved variables is

$$Q_c = a_L \left(q_w - q_{SAT}(T_L, p) \right) \tag{2.19}$$

and the local deviation from the mean is

$$s = a_L \left(q_w' - \alpha_L T_L' \right) \tag{2.20}$$

(a_L and α_L are defined by (2.14) and (2.15) above). The fluctuations represented here are not necessarily due to turbulence, as in Section 2.b, but rather to any unresolved motion.

The grid-box mean of s is zero since $\overline{q_w'}$ and $\overline{T_L'}$ are zero. The standard deviation of s is

$$\sigma_s = a_L \left(\overline{q_w'^2} - 2\alpha_L \overline{q_w' T_L'} + \alpha_L^2 \overline{T_L'^2} \right)^{1/2} \tag{2.21}$$

Higher order moments are similarly defined. The statistics of s are completely defined by its distribution function G.

Now the local cloud water content is

$$q_c' = \begin{cases} 0 & s \leq -Q_c \\ Q_c + s & s > -Q_c \end{cases} \tag{2.22}$$

The mean cloud fraction is obviously the fraction of the grid-box with cloud water content greater than zero. In terms of G,

$$C = \int_{-Q_c}^{\infty} G(s)\,ds \tag{2.23}$$

The grid-box mean cloud water content is similarly given by

$$q_c = \int_{-Q_c}^{\infty} (Q_c + s)G(s)ds \qquad (2.24)$$

To close the system G must be specified. Here a pragmatic choice is made: the symmetric triangular function with standard deviation σ_s shown in Figure 1. Evaluating the integrals on the r.h.s. of (2.23) and (2.24) with this G gives simple polynomial functions of Q_c and σ_s for the cloud fraction and water content (Appendix C).

The sub-gridscale fluctuations whose distribution are given by G are, in a large scale model, due not only to small scale turbulence but also to mesoscale effects. So using a higher order turbulence closure scheme to predict $\overline{q_w'^2}$ etc. is not appropriate for a grid-box large enough to contain other unresolved motions.

To examine the role of σ_s in the cloud scheme we set Q_c to the value at which cloud just forms, $-\sqrt{6}\sigma_s$ (see Appendix C), to obtain a threshold relative humidity for cloud,

$$RH_c = 1 - \frac{\sigma_s\sqrt{6}}{a_L q_{SAT}(T_L, p)} \qquad (2.25)$$

where the r.h.s. is evaluated for $q_c=0$, $T_L=T$ and $q_w=q=RH_c q_{SAT}(T, p)$. For RH_c to be a specifiable constant or function, without any temperature or pressure dependence determined by the q_{SAT} function, σ_s must have the form

$$\sigma_s = A a_L q_{SAT}(T_L, p) f\left(q_w/q_{SAT}(T_L, p)\right) \qquad (2.26)$$

where f is an arbitrary function. Substituting (2.26) into (2.25) gives

$$A = \frac{(1-RH_c)}{f(RH_c)\sqrt{6}} \qquad (2.27)$$

For simplicity $f=1$ has been chosen so that

$$\sigma_s = \frac{(1-RH_c)}{\sqrt{6}} a_L q_{SAT}(T_L, p) \qquad (2.28)$$

In the experiments reported below RH_c was set to 0.85 for all but the lowest two model layers where a value of 0.925 was used.

The cloud fraction C^+ given by the scheme is related to the relative humidity $RH^+ = q^+/q_{SAT}(T^+, p)$ (Appendix C). However, the cloud fraction is not calculated from the relative humidity as we do not know either until the cloud scheme has been used.

d. Layer cloud precipitation processes

Models which do not include a prognostic cloud water variable precipitate all condensed water as soon as it forms. A model with cloud water needs a parametrization of the depletion of cloud water due to precipitation. The scheme used is an adapted version of one used in a mesoscale weather forecasting model (Golding, 1986).

With the same notation as used in equation (2.1) the rate of conversion of cloud liquid water to precipitation is parametrized as:

$$(\dot{q}_L)_P = - C\left[c_T\left\{1 - \exp\left[-\left(\frac{q_L/C}{c_\omega}\right)^2\right]\right\} + c_A P\right]\frac{q_L}{C} \qquad (2.29)$$

The values used for the parameters in this expression are: $c_T = 10^{-4}\ s^{-1}$, $c_A = 1\ m^2\ kg^{-1}$ and $c_\omega = 8\times10^{-4}\ kg\ kg^{-1}$, as in the UK Meteorological Office mesoscale forecasting model (Golding, personal communication). P is the mass flux of precipitation entering the layer from above (after allowing for any evaporation).

Equation (2.29) is based on the parametrization proposed by Sundqvist (1978 and 1981) but with an additional accretion term $c_A P$ which increases the conversion rate when precipitation falls into a layer (Golding, 1986). Autoconversion of cloud droplets to rain is represented by the term involving c_T. The exponential factor in this term inhibits conversion when the in-cloud liquid water content is small compared with c_ω. The leading factor C is present because precipitation only forms in that fraction of the grid-box where there is cloud. The in-cloud mean liquid water content q_L/C is used rather than the grid-box mean. (The leading factor C and the final factor 1/C do of course cancel.)

There is in reality an important difference between liquid and ice clouds which the precipitation scheme incorporates. In water clouds the

available condensed water is spread over many cloud condensation nuclei (CCN) and few droplets are large enough to fall out (Pruppacher and Klett, 1978). Very few CCN act as ice nuclei (Heymsfield and Sabin, 1989), so cloud water in ice clouds is spread over fewer, larger particles, all of which quickly develop appreciable fall speeds (Heymsfield, 1977). A constant fall-out speed v_F of 1 m s^{-1} has been assumed for the parametrization of ice cloud precipitation. The flux of precipitation leaving a layer due to this cloud ice fallout is $\rho q_F v_F$. This implies, by taking the flux divergence across the layer, a rate of change of cloud ice water given by:

$$(\dot{q}_F)_F = P/\rho\Delta z - (v_F/\Delta z)q_F \qquad (2.30)$$

where Δz is the layer thickness and P is the frozen precipitation falling into the layer. Although for simplicity a constant v_F has been used, it would not be difficult make this a function of cloud ice content using the formula deduced from observations by Heymsfield (1977):

$$v_F = 3.23(\rho q_F)^{0.17}$$

The microphysics of mixed phase cloud are complex and not fully understood. Separate prognostic liquid water and ice content variables may be needed to represent the conversion processes in such cloud. A very simple approach has been used rather than introduce additional variables. Above 0°C all cloud water is assumed to be liquid and below -15°C all frozen. Between -15°C and 0°C the proportion of liquid cloud f_L in a grid-box is assumed to be given by a quadratic spline:

$$f_L = \begin{cases} 1/6\,((T+15)/5)^2 & \text{for } -15°C < T < -5°C \\ 1 - 1/3\,(T/5)^2 & \text{for } -5°C \leq T < 0°C \end{cases} \qquad (2.31)$$

giving a smooth transition between frozen and liquid states for the ensemble of clouds in a grid-box. For individual clouds in reality the transition is more abrupt and depends on factors other than local temperature such as cloud depth and cloud top temperature. All these

effects are intended to be represented by (2.31) for the ensemble. The form of the partitioning curve and the lower bound of -15°C for liquid water have no basis in observation or theory. The form was chosen for its simplicity and smoothness and the lower bound was chosen by "tuning". Excessive cloud was simulated if liquid water was assumed to exist below -15°C.

An alternative treatment of precipitation in the -15°C to 0°C temperature range has been adopted for the UKMO mesoscale weather prediction model (Golding, personal communication). This attempts to represent the glaciation for individual clouds while still retaining only one cloud water variable. In this scheme, where the cloud top is colder than -15°C all cloud colder than 0°C becomes ice; where the top is warmer the cloud is assumed to be supercooled liquid. This scheme is more appropriate for a model with high vertical and horizontal resolution.

The rates of change of specific humidity and temperature due to evaporation or sublimation of precipitation are parametrized as:

$$(\dot{q})_E = c_{EV}(q_{SAT}(T,p) - q)$$

$$(\dot{T})_E = -(L/c_p)(\dot{q})_E \qquad (2.32)$$

where $c_{EV} = 2\times10^{-5}\ s^{-1}$. Corresponding changes are made to the precipitation amounts.

The change in temperature due to melting or freezing of precipitation, $(\dot{T})_{MF}$, is calculated by assuming that the change of state takes place instantaneously and completely in the model layer containing the 0°C isotherm, as in the standard version of the model.

3. Results from a general circulation model including cloud water

The scheme described in the preceding section has been used in the Meteorological Office 11-layer finite difference AGCM. Brief details of the model specification are given in Tables 1, 2 and 4 of Slingo et al. (1988). The model has recently been coupled to an ocean GCM and sea-ice model (Foreman, 1986) but in the integration presented here the model had seasonally varying prescribed sea surface temperatures and sea-ice limits. The horizontal resolution was 2.5° latitude x 3.75° longitude and cloud optical properties were set to the values given in Table 1 of Slingo et al. (1988).

An integration of 15 months was done starting from September. The following sections present and assess the modelled cloud amount and water content distributions and the effects of the scheme on other aspects of the model simulation. Both model and observational data are displayed at a resolution of 5° latitude by 5° longitude. This is to ensure that the main features in the maps are not obscured by higher resolution detail.

a. Cloud cover

As reported by Slingo et al. (1988), the simulation of cloud cover by the Meteorological Office AGCM has been improved, particularly in the tropics and subtropics, by the introduction of changes to the detrainment in the convection scheme and to other parts of the model formulation. However, some deficiencies remained after these changes, especially in the low cloud field. In the winter season there was excessive low cloud over the northern hemisphere continents and the Arctic. Also the areas of subtropical oceanic stratocumulus did not extend far enough to the west away from the coasts of South America and southern Africa.

One of the reasons for the development of the scheme described in Section 2 was to improve the cloud cover simulation. This is an important aspect of an atmospheric model which can be coupled to ocean circulation and sea-ice models. Cloud cover over oceans and sea-ice modulates the net radiation at the surface. Also, through its effect on boundary layer turbulent and convective motions, low cloud affects the surface fluxes of sensible and latent heat. Thus a better cloud simulation should improve the simulated net surface heat flux which is imposed at the top boundary of

coupled ocean circulation and sea-ice models

Figures 2(a) and 2(b) show the mean total cloud cover simulated by the new scheme for December, January, February (DJF) and June, July, August (JJA) respectively. The global mean for the last 12 months of the simulation of total cloud cover is 0.53; this is made up of 0.25 low, 0.17 medium, 0.22 high and 0.095 convective with random overlap assumed between clouds at different levels. In northern winter, cloud cover over the cold land and Arctic sea-ice is realistic, exceeding 0.7 only over quite small areas. (Comparison in these regions can be made with the cloud climatology of Orvig and Vowinckel (1970).) In the summer over the Arctic, when the sea-ice is melting, the model's low cloud cover increases as it does in reality. Less realistic is the total cloud cover of more than 0.7 in the northwest of Canada and Alaska in JJA.

The improvement in the predicted winter low cloud in high latitudes is due to the rapid precipitation of cloud ice which was described in Section 2.d. This, combined with the fact that the scheme allows cloud water to form when the gridbox mean relative humidity is less than unity (but greater than RH_c), keeps the relative humidity and cloud fraction at realistic values less than unity. In an early development stage the scheme did not include a parametrization of the fallout of cloud ice water as distinct from that for liquid water. The low cloud over cold continents was then excessive, as was high cloud generally. It was these unrealistic results, as well as the desirability of treating precipitation from ice cloud in a more physically realistic way, which prompted the different treatment.

The mid-latitude depression belts in both the northern and southern hemispheres are clearly evident as areas of total cloud cover exceeding 0.7. Over subtropical oceans there is generally more low cloud than in the results obtained by Slingo et al. (1988) using the model without cloud water. There are also some areas of persistent low cloud particularly evident in the JJA cloud field off the coast of California and off the west coasts of South America and southern Africa. The area in the northern Pacific is positioned well but those in the southern hemisphere are not. In Fig. 2(b) the maximum southern subtropical oceanic cloud cover occurs at about 5-10°S and these areas are detached from the very low level (bottom model layer) cloud immediately adjacent to the coasts. Observations, such

as those analysed by Coulmann et al. (1986) and Saunders (1985), show that the extensive stratocumulus areas are further south and east and that there is little evidence of any gap between the coastal cloud and that further out where the boundary layer is deeper. This deficiency in the scheme's performance may be a consequence of not embedding a formulation of shallow convective mixing in the boundary layer scheme in a consistent and unified way. The modified turbulent mixing described in Section 2.b and the model's convection scheme are currently formulated and act independently. The work of Randall (1987) and Wang and Albrecht (1986) provide evidence that an updraught and downdraught convective circulation model should be included in a boundary layer mixing scheme.

b. Cloud water content

Figures 3(a) and 3(b) show the simulated distribution, for the DJF and JJA periods respectively, of the vertical integral through the whole atmosphere of cloud water content (the total cloud water path). As in the corresponding cloud cover maps (Figs. 2(a) and 2(b)) the mid-latitude depression tracks are clearly evident. There is an asymmetry in the peaks of cloud water path in mid-latitudes between the summer and winter hemispheres. The lower cloud water paths in the winter hemispheres are consistent with there being a higher proportion of cloud composed of frozen water. In the precipitation parametrization, frozen cloud water is removed from the atmosphere more rapidly than liquid water. The cloud water content is also likely to be less in colder regions even in the absence of precipitation processes (This point will be discussed more fully below). The low values of cloud water path in polar regions are also associated with low temperatures. During the warmer Arctic summer the cloud water path is considerably higher (but still less than in mid-latitudes). If the cloud radiative properties had been calculated rather than specified the albedo and longwave emissivity of the cloud in polar regions would have been lower because of their low optical depth.

Scanning Multichannel Microwave Radiometer (SMMR) measurements of the liquid water path over oceans (Prabhakara et al., 1983 and Njoku and Swanson, 1983) can be used for validation of the simulated values. Figure 4 shows the zonal mean of the simulated liquid water path for the JJA period as well as SMMR measurements taken from Njoku and Swanson (1983).

Only the liquid water paths zonally averaged over sea points are shown in this figure for both the simulation and observations (ice is transparent to microwaves at SMMR frequencies and data can only be retrieved over sea). In comparing the model results with observations in Figure 4 it should be borne in mind that the SMMR data include liquid water in convective cloud whereas the model's cloud water variable represents only that in layer cloud. This may explain the fact that the ITCZ peak in the simulation is less pronounced than in the observations. It is convective cloud which predominates in the ITCZ. However, the water detrained from convective towers can contribute to the layer cloud water path and this is what can be seen in the peak at about 6°N in Figure 4.

The zonal means of simulated cloud liquid water path compare quite well with SMMR observations: maxima occur in regions of large scale or sub-gridscale (convective) ascent and minima in the regions of subtropical subsidence. The model's cloud liquid water path has higher values than the SMMR observations in some areas particularly in the mid-latitudes of the summer hemisphere. This suggests that cloud liquid water is not being removed efficiently enough by the precipitation processes represented in the model. A modification to the scheme may be required to represent the enhanced precipitation efficiency of clouds in which ice crystals from cloud tops with temperatures less than -15°C "seed" the warmer lower parts of the clouds (this is discussed in 2.d).

The zonal means of the in-cloud water (liquid and ice) paths for high, medium and low clouds are shown in Figures 5(a), (b) and (c) respectively. The in-cloud water path is the appropriate quantity to use in any parametrization of cloud radiative properties. The range of the high cloud water paths is much smaller than that for medium and low cloud since this cloud is thin cirrus. The cirrus cloud water associated with the detrainment from deep convective clouds in the ITCZ can be seen in the peaks in Figure 5(a) at about 13°N and 13°S for the periods JJA and DJF respectively. The peaks at latitudes 30-40°N and S are further north in the northern summer (JJA). This is also a feature of the similarly positioned peaks in Figure 5(b) for the medium level in-cloud water paths. The medium level water paths at high latitudes have low magnitudes because the temperatures here are low and the clouds are composed largely of ice. The most marked feature of the low cloud water paths in Figure 5(c) is the

contrast between the summer and winter values in the northern middle and high latitudes. In winter the large area of cold land and, in polar regions, sea-ice leads to low clouds being cold and largely in the frozen state. In summer the warmer atmosphere can hold more water and low clouds which form are more likely to be in the liquid state and therefore precipitate less efficiently.

c. The relation of cloud water content to temperature

The instantaneous cloud water content at a given place will be related to many factors including temperature, pressure, vertical velocity, height above cloud base and the time and space scales of any turbulence and entrainment. A plot of observed or simulated cloud water contents against just one of these quantities such as temperature would therefore show a considerable degree of scatter. The observed data from the USSR analysed by Feigelson (1978) do indeed show this although the mean value of water content appears to be a function of temperature. This fact was used by Somerville and Remer (1984) to provide a simple parametrization of cloud water content and hence cloud optical properties in terms of temperature for their radiative-convective equilibrium climate model. Figure 6 shows a scatter plot, using model data, of the logarithm of in-cloud water content against temperature. The data are taken from a global field of the model valid at 00Z on day 20 of the December of the simulation. The most obvious feature of this diagram is the increase of $\ln(q_L/C)$ with temperature at least for temperatures less than about 270 K. The mean observed cloud water contents of Feigelson quoted by Somerville and Remer have also been plotted on Fig. 6. They are within the scatter of the simulated data points and the levelling off and then reversal of the gradient above freezing point is evident in both the observed and model data.

Betts and Harshvardhan (1987) have used moist thermodynamics to deduce the fractional change in liquid water content per degree temperature change at cloud base, f, assuming clouds have an adiabatic value for their water content. Their calculations show a considerable variation in f with pressure and temperature. f is always positive and increases rapidly as temperature decreases. With such a large scatter in Fig. 6 it is difficult to see if the gradient f changes much with temperature except near and above the freezing point. A straight regression line has been fitted to

the model data points below 268 K; its gradient is 0.096. This is more than twice the value deduced by Somerville and Remer from the observed data in the temperature range 248 K to 278 K. However it is in agreement with the adiabatic values for low temperatures (i.e. 248 K and below) deduced by Betts and Harshvardhan.

d. Earth's radiation budget

The model's radiation fields reflect many of the features of the simulated cloud fields discussed above. However, the simulated shortwave planetary albedo and the Outgoing Longwave Radiation (OLR) fields are more directly verifiable using satellite Earth Radiation Budget (ERB) measurements than are the cloud fields. Data from the Nimbus 7 ERB experiment (Kyle et al., 1985) are compared here with model fields. The narrow field of view data with calibration corrections are used as in Slingo et al. (1988).

Figures 7(a) and 7(b) show the Nimbus 7 and model OLR fields respectively for DJF and Figures 8(a) and 8(b) show the same for JJA. The observed and simulated fields are generally in close agreement. However, some discrepancies are evident: the model gives too low OLR values over Alaska, northwest Canada and northern Eurasia in JJA and the areas over subtropical oceans with OLR above 275 W m^{-2} are more extensive than in reality particularly in JJA. The low OLR in high northern latitudes in JJA is associated with excessive cloud and the high values in the subtropics suggest too little high cloud. The annual, global mean OLR emission from the model is 234.7 W m^{-2} which is close to the Nimbus 7 value of 235.8 W m^{-2}.

Figures 9(a) and 9(b) show the Nimbus 7 and model shortwave planetary albedo fields respectively for DJF and Figures 10(a) and 10(b) show the same for JJA. Excess cloud in northern Eurasia and northwestern North America in JJA results in the area with albedo greater than 0.4 extending too far south in the model's fields. The errors in the position of the subtropical oceanic stratocumulus off the west coasts of South America and southern Africa can be seen in the albedo field. Despite these shortcomings the simulated albedo field has many realistic features although the annual global mean of 0.313 is somewhat greater than the observed value of 0.302.

e. Precipitation

The method of calculating the large-scale precipitation presented in Section 2.d is clearly very different to the usual procedure of precipitating all the condensate which forms to remove supersaturation. It is therefore of interest to look at the precipitation field produced by the new scheme. The mean distribution of total precipitation for DJF is shown in Figure 11(b). The climatological precipitation data of Jaeger (1983) for the same period are shown in Figure 11(a) for comparison. There is reasonable agreement between the model results and the observed data. In some respects, most notably the almost continuous Atlantic ITCZ rainbelt, the results are better than those produced by the standard version of the model (Slingo et al., 1988). However, in most areas the use of the new scheme makes very little difference to the total precipitation field. This is perhaps unsurprising if the model's large-scale precipitation distribution, when meaned over extended periods, is determined by the circulation in the model. This view is supported by the observation that the time-meaned precipitation changed little when the rate parameter for conversion of cloud water to precipitation was changed in early development studies of the scheme. Such changes have a much larger effect on the mean cloud amount and water content than on the total amount of precipitation.

4. Discussion

It has been shown that the introduction of a predicted cloud water variable in an AGCM has several benefits. From a theoretical viewpoint the cloud water enables some of the components of the model's physical processes, previously formulated independently or with no explicit regard to cloud, to be reformulated in a more consistent way. Thus the hydrological cycle is directly related to the cloud used for the calculation of radiative fluxes and boundary layer mixing. The results from the scheme are encouraging. The predicted cloud amounts are better than those produced by the model's standard cloud prediction scheme and there are associated improvements in the simulated radiation fields. The predicted cloud water content agrees well with the limited amount of observational data so far published.

The realistic cloud water content of the model gives hope that the next step in this work, the interactive calculation of cloud radiative

properties, will likewise produce physically reasonable results. The model will then be general enough to be used for calculating the feedbacks due to cloud radiative property changes as well as cloud distribution changes in climate perturbation experiments.

So far, verification of the model's cloud and radiation against observed climatologies has been for time averaged fields. Comparison of the scheme's cloud predictions with observations would be useful when it is used in a forecast model. Further assessment and refinement of the scheme should also be aided by data from the International Satellite Cloud Climatology Project (ISCCP) experiments. Assessment of model simulations using ISCCP cloud climatologies can and should be made on regional as well as global scales and on shorter timescales than has been usual. The data derived from satellite measurements in the ISCCP is at three hourly intervals and so will allow verification of diurnal variations as well as time means. Attention should be directed particularly to specific cloud types where uncertainties or known inadequacies in the cloud scheme exist. The development of the parametrization of boundary layer processes in marine stratocumulus and shallow trade-wind cumulus regions should be particularly influenced by what is learnt from the First ISCCP Regional Experiment (FIRE) (Cox et al., 1987). This an aspect of the scheme already identified as requiring improvement from the simulation results presented above.

Acknowledgements

I am grateful to David Pearson for his help in coding the scheme and to Joe Lavery and Stuart Brentnall for assistance in producing diagnostics and diagrams. William Ingram provided some detailed comments on a draft of the text which helped clarify it. Thanks are also due to Malcolm MacVean who pointed out the relevence of his and Paul Mason's recent work on cloud top entrainment instability to defining the Richardson number.

Appendix A

The functions of stability f_H and f_M introduced in Section 2b for calculating the turbulent transport coefficients are specified as:

$$f_H = f_M = 1.6875/(1+40Ri) \qquad 0.05 \leq Ri$$

$$f_H = f_M = (1-5Ri)^2 \qquad 0 \leq Ri < 0.05$$

$$\left.\begin{aligned} f_H &= 1 - 10Ri/(1+0.4(-Ri)^{1/2}) \\ f_M &= 1 - 10Ri/(1+2.5(-Ri)^{1/2}) \end{aligned}\right\} \qquad Ri < 0$$

f_H and f_M and their first derivatives are continuous. These are not precisely the same as the stability functions previously used (Mitchell and Slingo, 1988). In the very stable limit the functions become very small but no longer reduce to zero and cut off all mixing. In the opposite highly unstable limit both f_M and f_H vary as $(-Ri)^{1/2}$. Near neutrality, where most of the empirical data are available, the functions differ very little from those previously used.

Appendix B

The finite-difference form of the Richardson number defined in (2.11) can be written:

$$Ri = g\Delta z\left[(W_1\tilde{\beta}_{T1}+W_2\tilde{\beta}_{T2})(\Delta T_L+g\Delta z/c_p) + (W_1\tilde{\beta}_{Q1}+W_2\tilde{\beta}_{Q2})\Delta q_w\right]/|\Delta u|^2 \qquad (B.1)$$

where the subscripts 1 and 2 refer to the layers below and above the interface respectively, Δz is the mid-layer separation, i.e. z_2-z_1, and W_1 and W_2 $(=1-W_1)$ are the weights for the layers. Values of the weights can be derived from the energetic stability analysis as described by Mason (1985) and as used by MacVean and Mason (personal communication) in an analysis of cloud-top entrainment instability through small-scale mixing.. A small mass of air ε_M is exchanged between the layers and mixed. The resulting changes in potential and kinetic energies of the two layers per unit mass exchanged are calculated. The Richardson number can be defined in terms of these energy changes as

$$Ri = - \frac{\delta PE/\varepsilon_M}{\delta KE/\varepsilon_M} \qquad (B.2)$$

where δ represents the change due to the mixing of mass ε_M and PE and KE are the potential and kinetic energies respectively. For small ε_M this quantity drops out of the expression for Ri and (B.1) is obtained with

$$W_1 = \Delta z_1/2\Delta z \qquad \text{and} \qquad W_2 = \Delta z_2/2\Delta z \qquad (B.3)$$

Δz_1 and Δz_2 are the lower and upper layer thicknesses respectively. These are the weights which have been used in the scheme.

The Richardson number given by (B.1) implies instability if

$$\Delta h < k_M L \Delta q_\omega \qquad (B.4)$$

where $h = c_p T + Lq + gz$ is the moist static energy

and $$k_M = 1 - \frac{c_p}{L} \frac{(W_1\tilde{\beta}_{q1} + W_2\tilde{\beta}_{q2})}{(W_1\tilde{\beta}_{T1} + W_2\tilde{\beta}_{T2})} \qquad (B.5)$$

Substituting for the buoyancy parameters $\tilde{\beta}$ from (2.12) in (B.5) we obtain

$$k_M = \frac{\{N_1 - N_2(c_p T/L)\}(1+L\alpha/c_p)}{\{D_1 + D_2(1+\delta)\alpha T\}} \qquad (B.6)$$

where

$$N_1 = [W_1(1-C_1) + W_2(1-C_2)], \qquad N_2 = [W_1(\delta - C_1(1+\delta)) + W_2(\delta - C_2(1+\delta))],$$

$$D_1 = W_1[1+(L\alpha/c_p)(1-C_1)] + W_2[1+(L\alpha/c_p)(1-C_2)], \qquad D_2 = [W_1C_1 + W_2C_2],$$

$\alpha = \partial q_{sAT}/\partial T$, $\delta = 0.608$, T is the mean of T_1 and T_2 and C_1 and C_2 are cloud fractions.

Putting $C_1 = C_2 = 1$ in (B.6), $k_M = k_\omega$ where

$$k_\omega = \frac{(c_p T/L)(1+L\alpha/c_p)}{[1+(1+\delta)\alpha T]} \qquad (B.7)$$

In this case the weights drop out of the expression for k_M and the instability criterion (B.4) is that derived by Randall (1980) and Deardorff (1980) for cloud top entrainment instability (CTEI). However, MacVean and Mason (personal communication) argue that the appropriate criterion for CTEI is that which is obtained by putting $C_1=1$ and $C_2=0$ giving

$$k_M = \frac{\{c_p T/L + (W_2/W_1)(1-c_p T\delta/L)\}(1+L\alpha/c_p)}{\{(1+W_2/W_1) + [(W_2/W_1)L/c_p T + (1+\delta)]\alpha T\}} \qquad (B.8)$$

MacVean and Mason also argue that "a self-sustaining dynamical instability is most likely when the two layers involved in the mixing process are of comparable depth". This implies that the weights should be equal for a correct calculation of stability across cloud top. In fact the UKMO AGCM, like other large-scale models, has layer thicknesses increasing with height in the boundary layer so that there is a greater weighting for the upper layer (i.e. $W_2>W_1$). This biasses the stability parameter k_M given by (B.8) towards its dry mixing value $k_D = 1 - c_p T\delta/L$, obtained by putting $C_1=C_2=0$ in (B.6). This can be seen by noting that the dry value is also obtained in the limit $W_2/W_1 \to \infty$ in (B.8). (It is also worth noting that k_ω is obtained in the limit $W_2/W_1 \to 0$ in (B.8)).

For T=288 K, $k_D=0.93$, $k_\omega=0.23$ and, for $W_1=W_2$, (B.8) gives $k_M=0.70$. Since Δq_ω is negative for an inversion, the bias in the model to the dry mixing instability criterion tends to inhibit CTEI. However, the model does not show an unrealistic overpersistence of stratocumulus layers (Section 3a) because the penetrative convection scheme mixes some boundary layer air with air above the inversion (Slingo et al., 1989).

Appendix C

The cloud fraction and water content derived assuming the triangular distribution function with standard deviation σ_s are given in terms of Q_c and σ_s by:

$$C = \begin{cases} 0 \\ \frac{1}{2}(1+Q_N/\sqrt{6})^2 \\ 1-\frac{1}{2}(1-Q_N/\sqrt{6})^2 \\ 1 \end{cases} \qquad q_c/\sigma_s = \begin{cases} 0 & Q_N \leq -\sqrt{6} \\ (1+Q_N/\sqrt{6})^3/\sqrt{6} & -\sqrt{6} < Q_N \leq 0 \\ Q_N+(1-Q_N/\sqrt{6})^3/\sqrt{6} & 0 < Q_N < \sqrt{6} \\ Q_N & \sqrt{6} \leq Q_N \end{cases}$$

where $Q_N = Q_c/\sigma_s$.

The cloud fraction can be written in terms of the grid-box mean relative humidity, $RH=q/q_{SAT}(T,p)$, which is calculated using the cloud conserved variables and the q_c given above.

For $RH \leq RH_c$,

$$C = 0;$$

for $RH_c < RH < (5+RH_c)/6$, $C=\frac{1}{2}R^2$ where R satisfies

$$R^3 - 6R + 6\left[\frac{RH-RH_c}{1-RH_c}\right] = 0;$$

the physically realistic root of this cubic gives

$$C = 4\cos^2(\pi/3 + \varphi/3) \quad \text{where} \quad \varphi = \cos^{-1}\left[\frac{3}{2\sqrt{2}}\left(\frac{RH-RH_c}{1-RH_c}\right)\right];$$

for $(5+RH_c)/6 \leq RH \leq 1$,

$$C = 1 - \left[\frac{3}{\sqrt{2}}\left(\frac{1-RH}{1-RH_c}\right)\right]^{2/3}.$$

References

Betts, A. K. and Harshvardhan, 1987: Thermodynamic constraint on the cloud liquid water feedback in climate models. J. Geophys. Res. **92**, 8483-8485.

Coulmann, S., Bakan, S. and Hinzpeter, H., 1986: A cloud climatology for the South Atlantic derived from METEOSAT I images. Tellus, **38A**, 453-461.

Cox, S. K., McDougal, D. S., Randall, D. A. and Schiffer, R. A., 1987: FIRE - The first ISCCP regional experiment. Bull. Amer. Met. Soc., **68**, 114-118.

Deardorff, J. W., 1980: Cloud top entrainment instability. J. Atmos. Sci., **37**, 131-147.

Feigelson, E. M., 1978: Preliminary radiation model of a cloudy atmosphere, 1, Structure of clouds and solar radiation. Beitr. Phys. Atmos., **51**, 203-229.

Foreman, S. J., 1986: Ocean and atmosphere interact! Meteorol. Mag., **115**, 358-361.

Geleyn, J.-F., 1981: Some diagnostics of the cloud-radiation interaction in the ECMWF forecast model. Workshop on radiation and cloud-radiation interaction in numerical modelling, 15-17 October 1980. ECMWF Reading, 135-162.

Golding, B. W., 1986: Short range forecasting over the United Kingdom using a mesoscale forecasting system. Short- and Medium-Range Numerical Weather Prediction. Collection of papers presented at the WMO/IUGG NWP Symposium, Tokyo, 4-6 August 1986. (Ed. Matsuno, T.) Met. Soc. of Japan. 563-572

Golding, B. W., 1987: The U. K. Meteorological Office mesoscale model. Boundary Layer Meteor., **41**, 97-107.

Hense, A. and Heise, E., 1984: A sensitivity study of cloud parametrizations in general circulation models. Beitr. Phys. Atmos., **57**, 240-258.

Heymsfield, A. J., 1977: Precipitation development in stratiform ice clouds: a microphysical and dynamical study. J. Atmos. Sci., **34**, 367-381.

Heymsfield, A. J. and Sabin, R. M., 1989: Cirrus crystal nucleation by homogeneous freezing of solution droplets. J. Atmos. Sci., **46**, 2252-2264

Jaeger, L., 1983: Monthly and areal patterns of mean global precipitation. Variations in the global water budget. D. Reidel Publishing Company.

Kyle, H. L., Ardanuy, P. E. and Hurley, E. J., 1985: The status of the Nimbus-7 earth radiation budget data. Bull. Amer. Met. Soc., **66**, 1378-1388.

Le Treut, H., 1985: Cloud prediction experiments with the LMD GCM. Workshop on cloud cover parametrization in numerical models, 26-28 November 1984. ECMWF Reading, 65-86.

Mason, P. J., 1985: A numerical study of cloud streets in the planetary boundary layer. Bound. Layer Meteorol., **32**, 281-304.

Mellor, G. L., 1977: The Gaussian cloud model relations. J. Atmos. Sci., **34**, 356-358, 1483-1484.

Mellor, G. L. and Yamada, T., 1982: Development of a turbulence closure model for geophysical flows. Rev. Geophys. and Space Phys., **20**, 851-875.

Mitchell, J. F. B. and Slingo, A., 1988: Climatic effects of nuclear war: the role of atmospheric stability and ground heat fluxes. J. Geophys. Res. **93**, 7037-7045.

Njoku, E. G. and Swanson, L., 1983: Global measurements of sea surface temperature, wind speed and atmospheric water content from satellite microwave radiometry. Mon. Wea. Rev., **111**, 1977-1987.

Orvig, S. and Vowinckel, E., 1970: The climate of the north polar basin. Chapter 3 of "Climates of the Polar Regions" edited by Orvig, S. in World Survey of Climatology, Volume 14; Elsevier Publishing Company.

Prabhakara, C., Wang, I., Chang, A. T. C. and Gloersen, P., 1983: A statistical examination of Nimbus-7 SMMR data and remote sensing of sea surface temperature, liquid water content in the atmosphere and surface wind speed. J. Clim. and Appl. Meteorol., **22**, 2023-2037.

Pruppacher, H. R. and Klett, J. D., 1978: Microphysics of cloud and precipitation. Dordrecht, D. Reidel Publ. Co.

Randall, D. A., 1980: Conditional instability of the first kind upside-down. J. Atmos. Sci., **37**, 125-130.

Randall, D. A., 1987: Turbulent fluxes of liquid water and buoyancy in partly cloudy layers. J. Atmos. Sci., **44**, 850-858.

Roeckner, E. and Schlese, U., 1985: January simulation of clouds with a prognostic cloud cover scheme. Workshop on cloud cover parametrization in numerical models, 26-28 November 1984. ECMWF Reading, 87-108.

Roeckner, E., Schlese, U., Biercamp, J. and Loewe, P., 1987: Cloud optical depth feedbacks and climate modelling. Nature **329**, 138-140.

Rogers, D. P., Businger, J. A. and Charnock, H., 1985: A numerical investigation of the JASIN atmospheric boundary layer. Boundary Layer Meteor., **32**, 373-399

Sasamori, T., 1975: A statistical model for stationary atmospheric cloudiness, liquid water content and rate of precipitation. Mon. Wea. Rev. **103**, 1037-1049.

Saunders, R. W., 1985: Monthly mean cloudiness from METEOSAT-2. J. Clim. and Appl. Meteor., **24**, 114-127.

Schlesinger, M. E., 1988: Negative or positive cloud optical depth feedback? Nature, **335**, 303-304.

Slingo, A. (Editor), 1985: Handbook of the Meteorological Office 11-layer atmospheric general circulation model. Volume 1: Model description. Available on request from the Dynamical Climatology Branch, Meteorological Office, Bracknell, Berkshire, U.K.

Slingo, A., Wilderspin, R. C. and Smith, R. N. B., 1989: The effect of improved parametrizations on simulations of cloudiness and the earth's radiation budget in the tropics. J. Geophys. Res., **94**, 2281-2302.

Slingo, J. M., 1987: The development and verification of a cloud prediction scheme for the ECMWF model. Q. J. R. Meteorol. Soc., **113**, 899-927.

Somerville, R. C. J. and Remer, L. A., 1984: Cloud optical thickness feedbacks in the CO_2 climate problem. J. Geophys. Res. **89**, 9668-9672.

Somerville, R. C. J. and Iacobellis, S., 1987: Cloud-radiation interactions: Effects of cirrus optical thickness feedbacks. Collection of papers presented at the WMO/IUGG symposium on short and medium range numerical weather prediction, Tokyo, 4-8 August 1986, 177-185.

Sommeria, G. and Deardorff, J. W., 1977: Subgrid-scale condensation in models of non-precipitating clouds. J. Atmos. Sci., **34**, 344-355.

Sundqvist, H., 1978: A parametrization scheme for non-convective condensation including prediction of cloud water content. Q. J. R. Meteorol. Soc., **104**, 677-690.

Sundqvist, H., 1981: Prediction of stratiform clouds: results from a 5-day forecast with a global model. Tellus, **33**, 242-253.

Wang, S. and Albrecht, B. A., 1986: A stratocumulus model with an internal circulation. J. Atmos. Sci., **43**, 2374-2391.

Yamada, T. and Mellor, G. L., 1979: A numerical simulation of BOMEX data using a turbulence closure model coupled with cloud ensemble relations. Q. J. R. Meteorol. Soc., **105**, 915-944.

FIGURE CAPTIONS

Figure 1 The symmetric triangular probability distribution function with standard deviation σ_s used in the cloud model.

Figure 2 The total cloud amount simulated by the AGCM with the cloud water scheme, (a) for DJF and (b) for JJA. The contour interval is 0.2 and areas with values greater than 0.5 are shaded.

Figures 3(a) and (b) As Figs. 2(a) and (b) respectively but for the cloud water path through the whole atmosphere. The contours are at 10, 50, 100, 200, 300 and 400 g m^{-2} and areas with values above 100 g m^{-2} are shaded.

Figure 4 The variation with latitude of the zonal mean cloud liquid water path over oceans in g m^{-2}. The dashed line follows the SMMR data for the period 11 July to 10 August, the dotted line for the period 11 September to 10 October 1978 from Njoku and Swanson (1983) and the solid line is the JJA mean from the model simulation.

Figure 5 The simulated variation with latitude of the zonal mean in-cloud water paths in g m^{-2} for (a) high cloud, (b) medium level cloud and (c) low cloud. (Note the different vertical scales.) The solid lines show the DJF values and the dashed lines those for JJA.

Figure 6 A plot of the logarithm of in-cloud water content against temperature. Data points are taken from an instantaneous model field (00Z on day 20, December). The line is a least squares linear fit to the points with temperatures less than 268 K and has gradient 0.096. The observed data presented by Feigelson (1978) are shown as ⊕.

Figure 7 Outgoing longwave radiation in W m^{-2} for DJF (a) derived from Nimbus 7 narrow field of view data for 1979/80 and (b) simulated by the model. The contour interval is 25 W m^{-2} and areas with values below 225 W m^{-2} are shaded.

Figures 8(a) and (b) As Figs. 7(a) and (b) respectively but for JJA.

Figure 9 Shortwave planetary albedo as a percentage for DJF, (a) derived from Nimbus 7 narrow field of view data for 1979/80 and (b) simulated by the model. The contour interval is 10% and areas with values greater than 30% are shaded.

Figures 10(a) and (b) As Figs. 9(a) and (b) respectively but for JJA.

Figure 11 The total precipitation for DJF in mm day^{-1}, (a) the data of Jaeger (1983) and (b) as simulated by the model. The contours are at 0, 0.1, 1, 2, 5, 10 mm day^{-1} and areas with values greater than 5 mm day^{-1} are shaded.

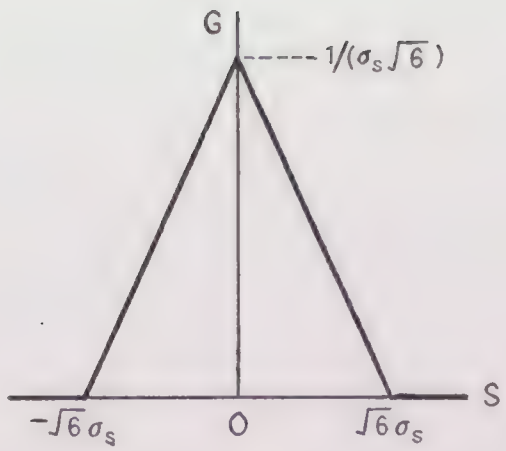

FIGURE 1

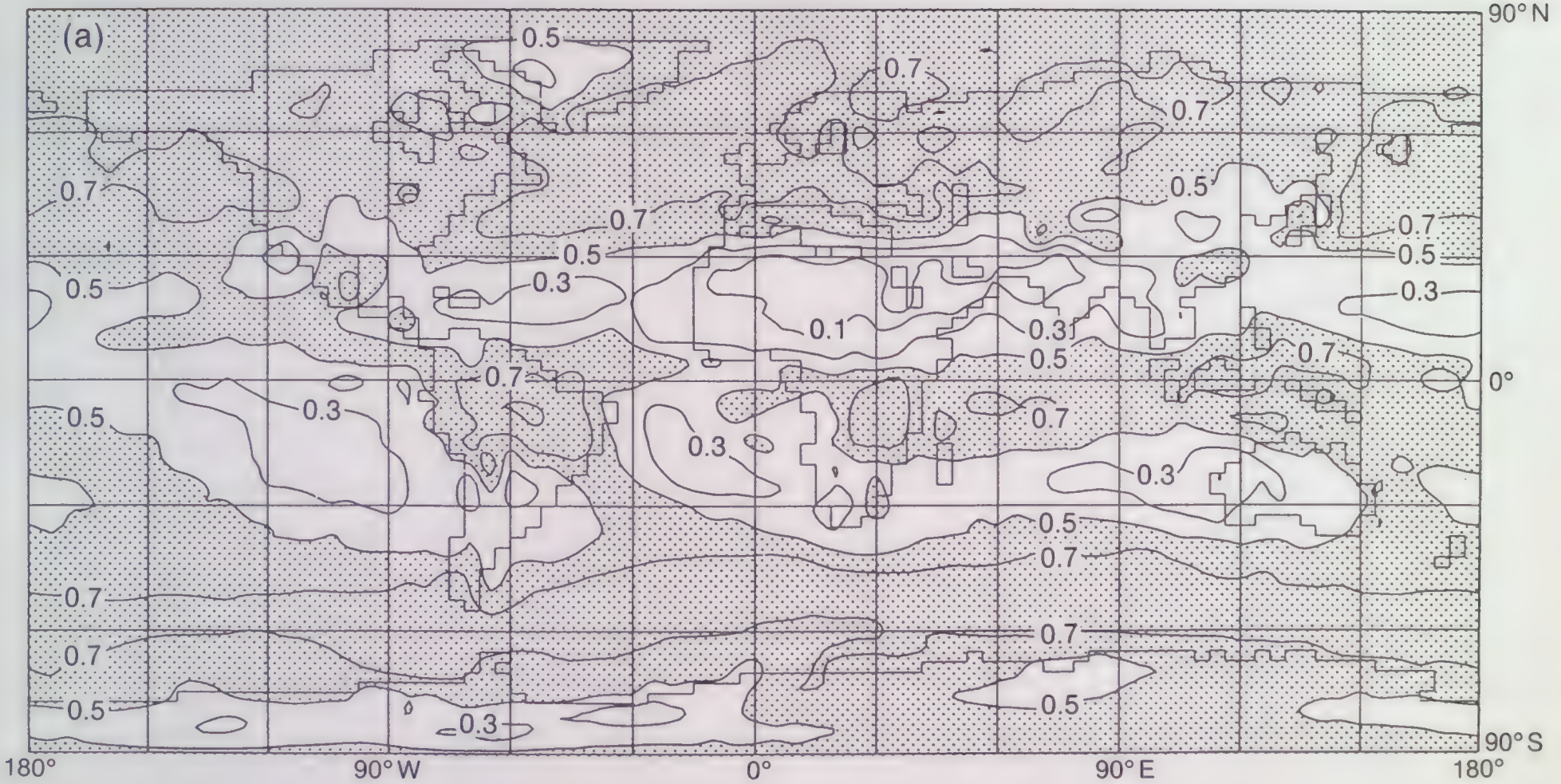

Figure 2 (a)

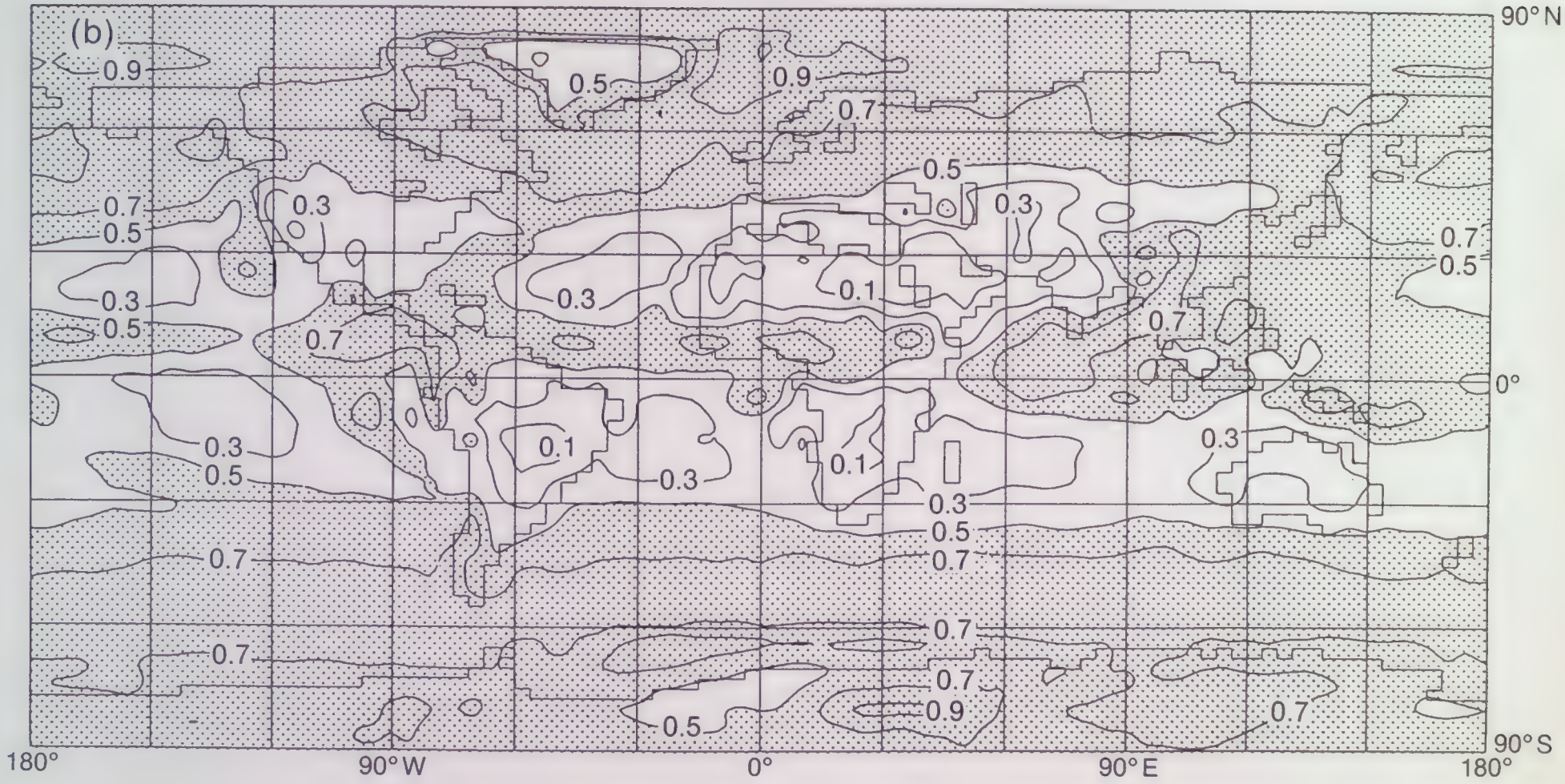
(b)
90° N
0°
90° S
180°
90° W
0°
90° E
180°
0.9
0.5
0.9
0.7
0.5
0.7
0.3
0.3
0.5
0.3
0.1
0.7
0.5
0.7
0.3
0.5
0.7
0.1
0.1
0.3
0.3
0.5
0.7
0.7
0.7
0.7
0.9
0.5
0.7

Figure 2(b)

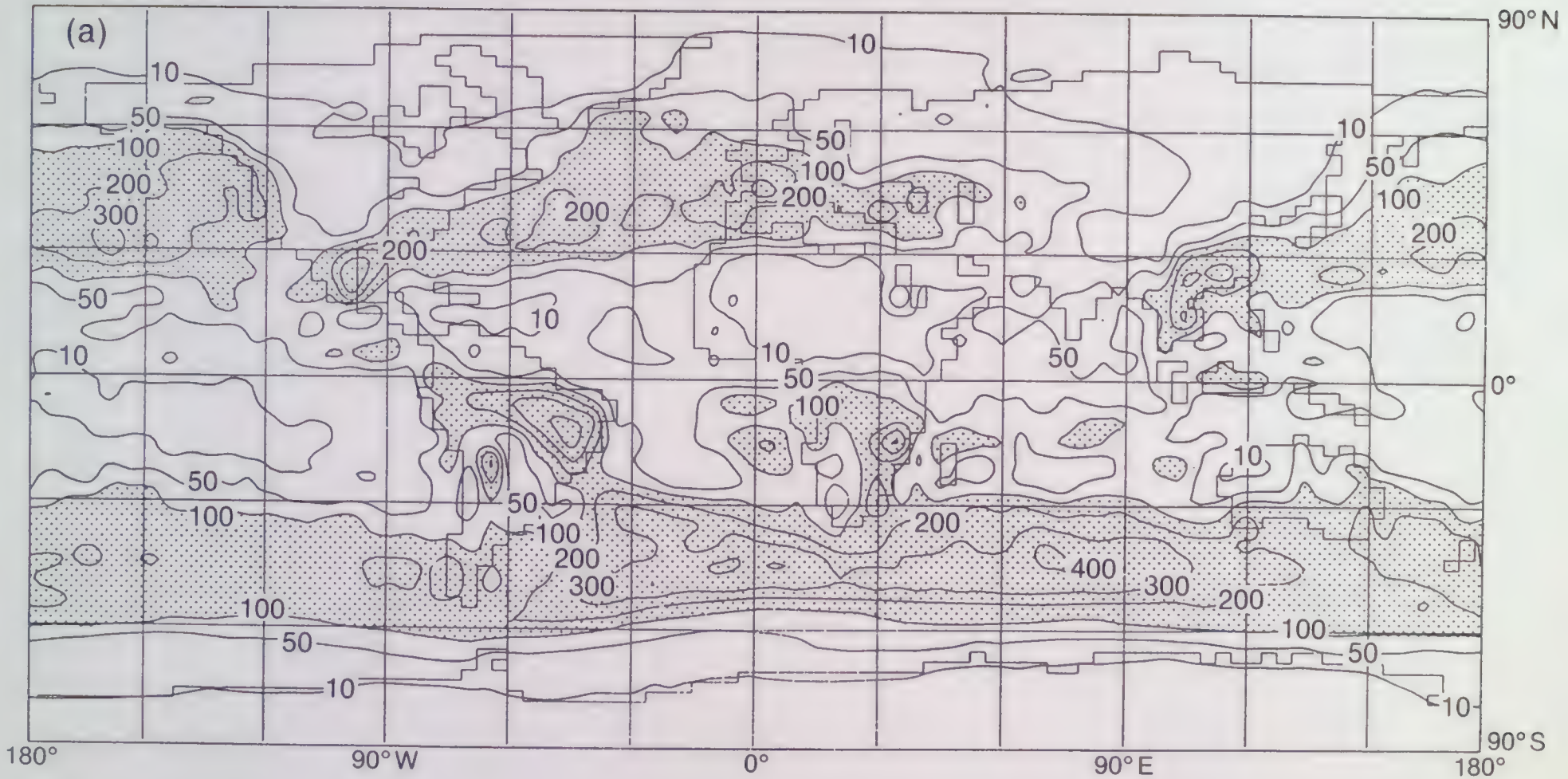

Figure 3(a)

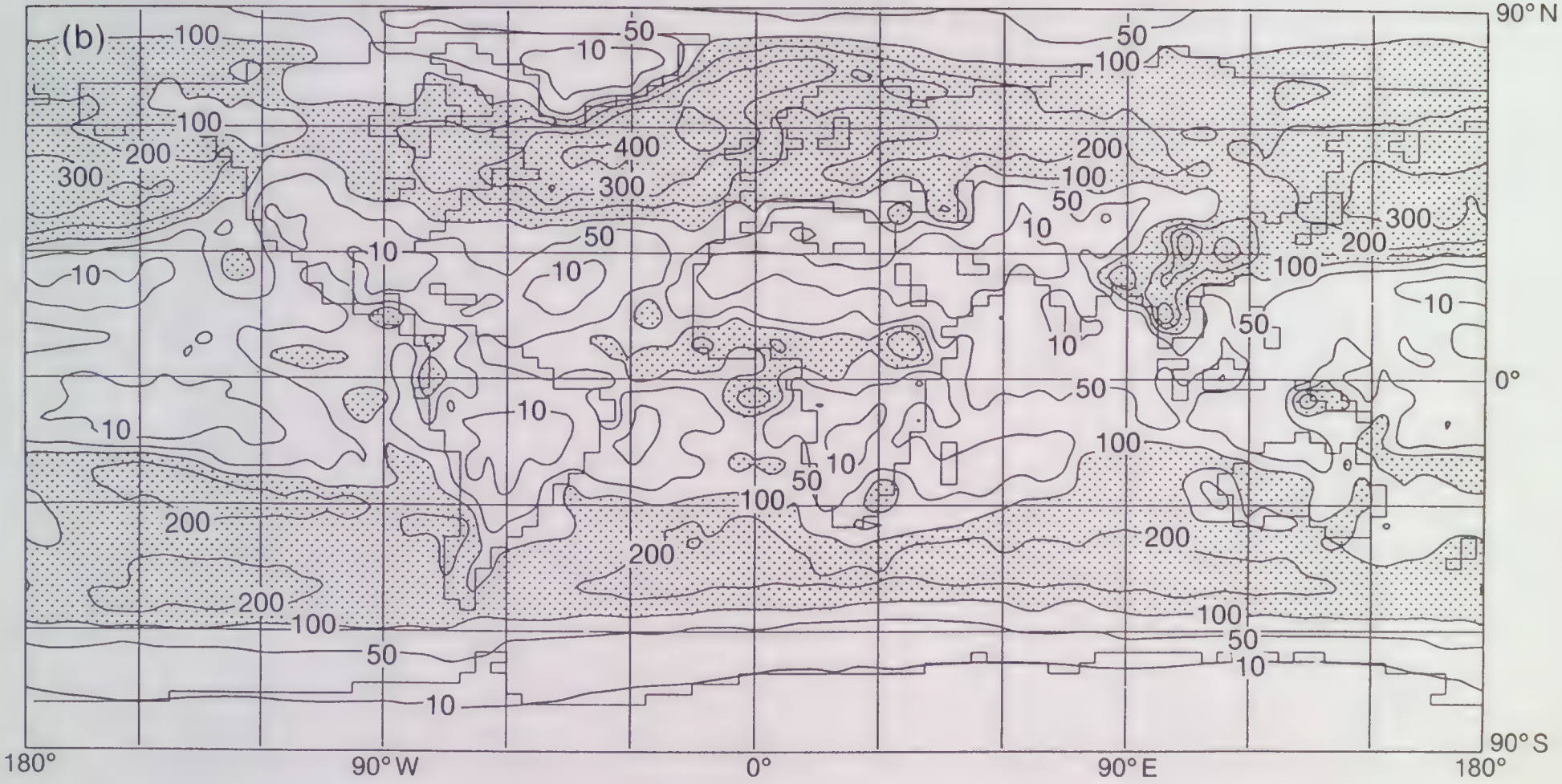

Figure 3(b)

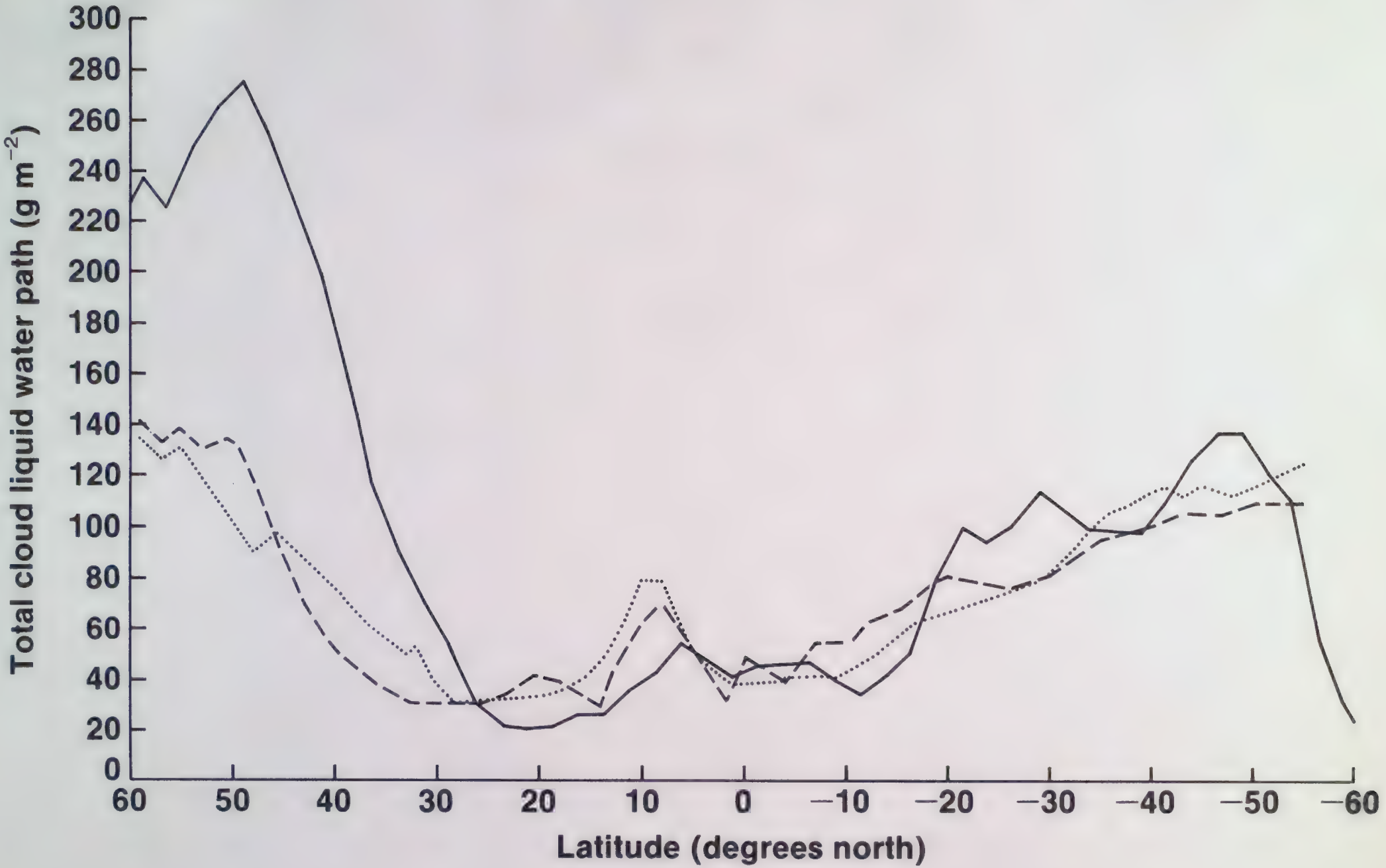
Total cloud liquid water path (g m^{-2})
300
280
260
240
220
200
180
160
140
120
100
80
60
40
20
0
60
50
40
30
20
10
0
−10
−20
−30
−40
−50
−60
Latitude (degrees north)

Figure 4

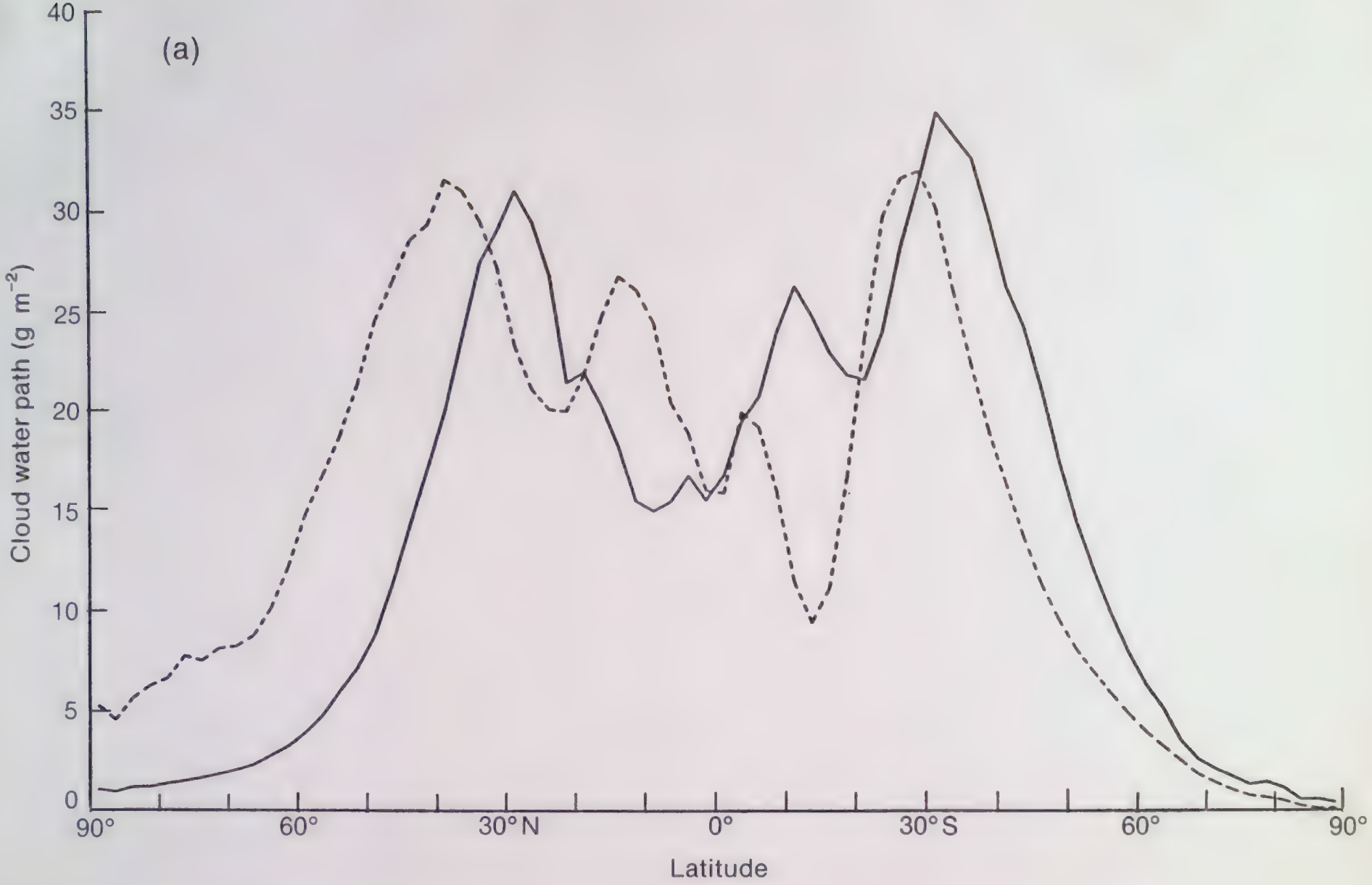
(a)
40
35
30
25
20
15
10
5
0
Cloud water path (g m^{-2})
90°
60°
30° N
0°
30° S
60°
90°
Latitude

Figure 5(a)

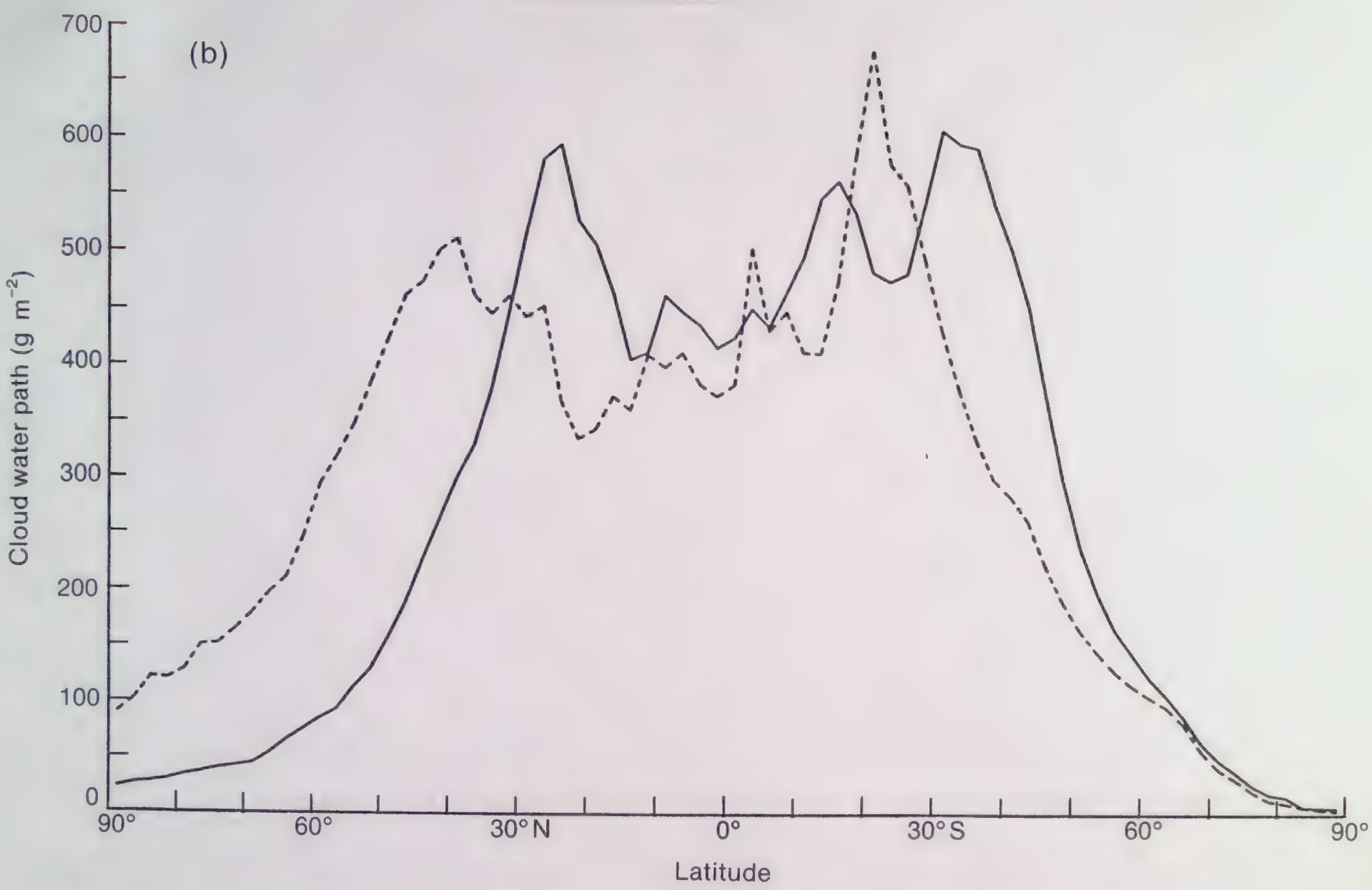
(b)
700
600
500
400
300
200
100
0
Cloud water path (g m^{-2})
90°
60°
30° N
0°
30° S
60°
90°
Latitude

Figure 5(b)

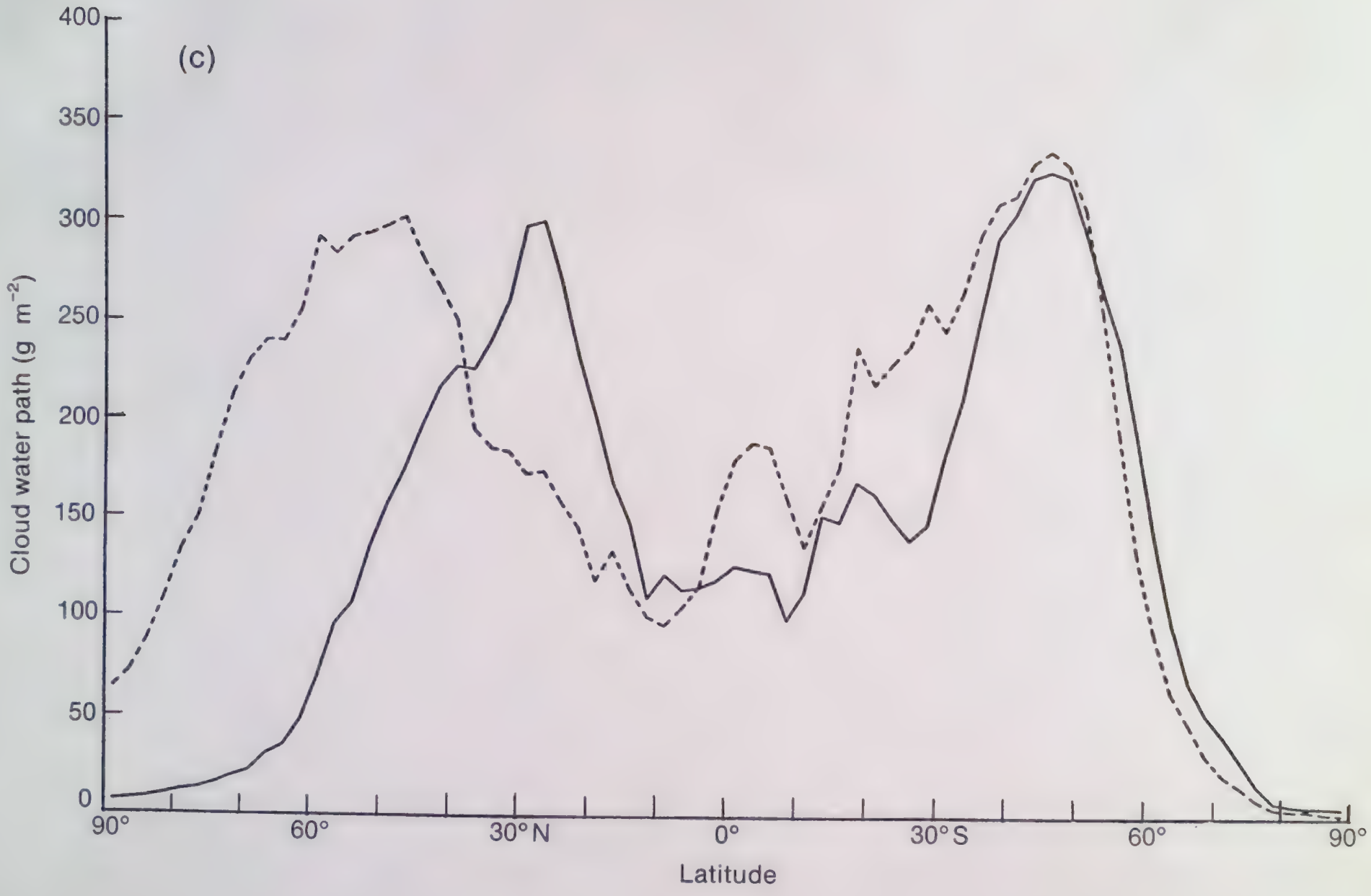
(c)
400
350
300
250
200
150
100
50
0
Cloud water path (g m^{-2})
90°
60°
30° N
0°
30° S
60°
90°
Latitude

Figure 5(c)

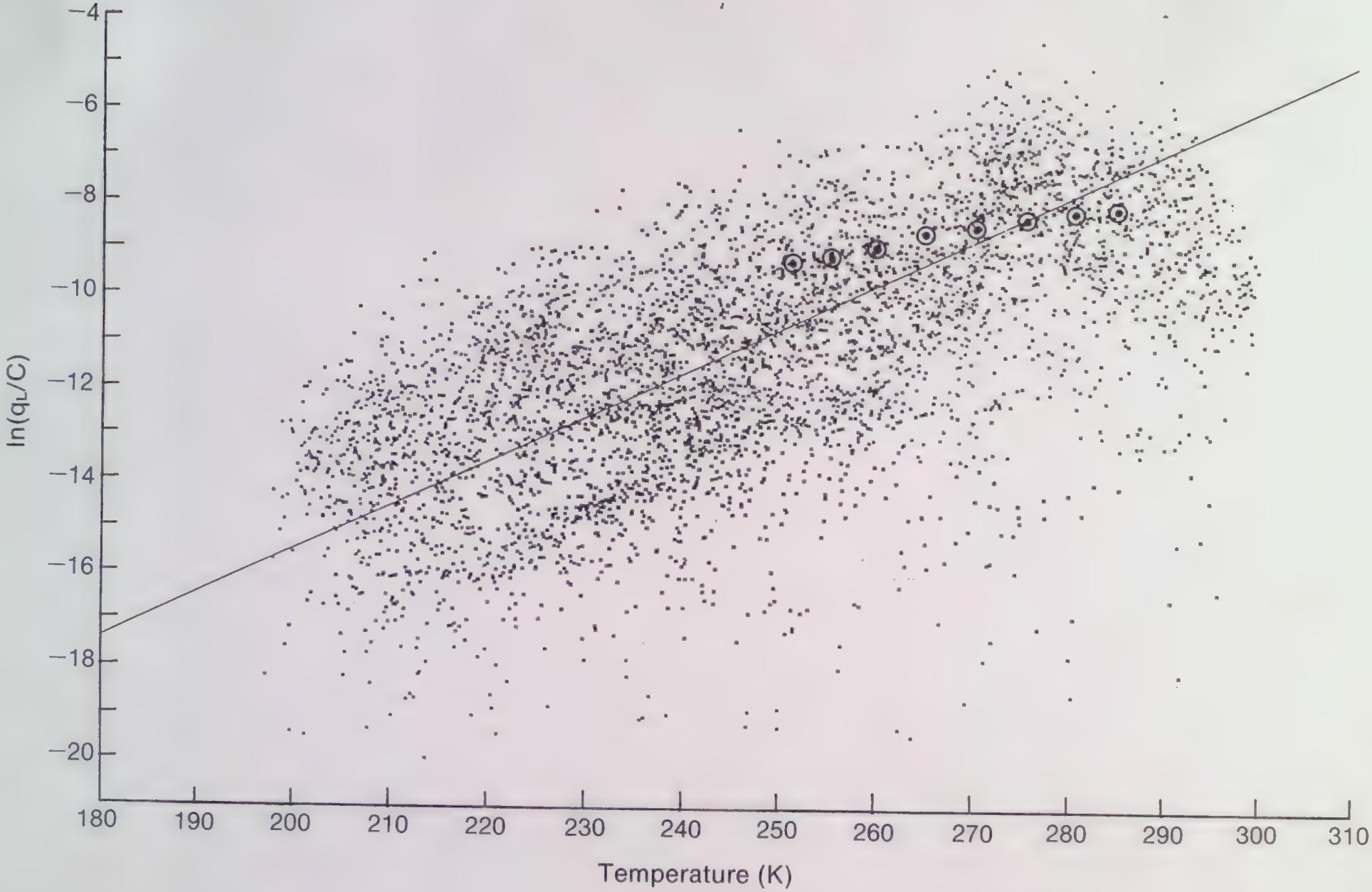
−4
−6
−8
−10
−12
−14
−16
−18
−20
ln(qL/C)
180
190
200
210
220
230
240
250
260
270
280
290
300
310
Temperature (K)

Figure 6

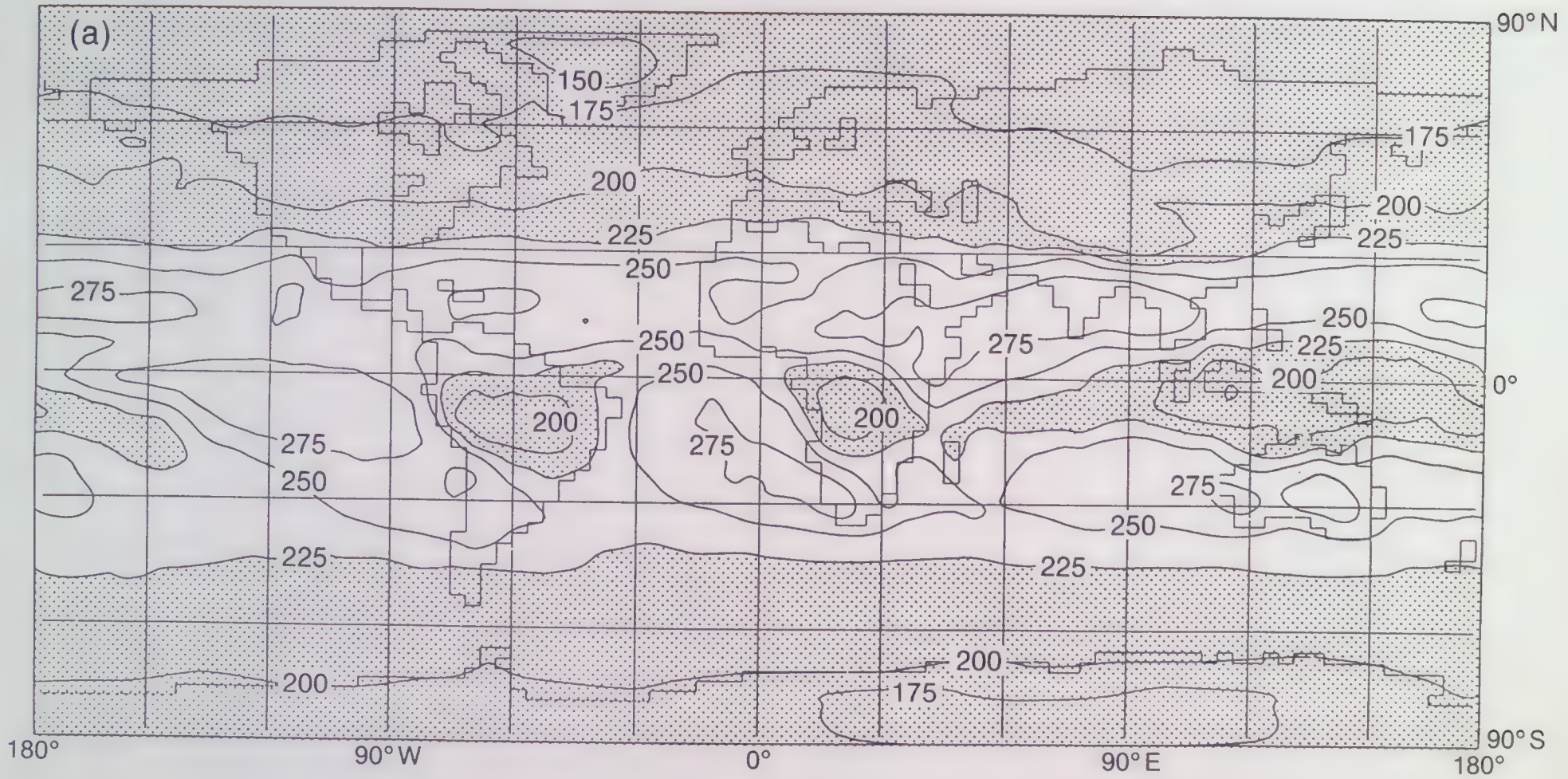

Figure 7(a)

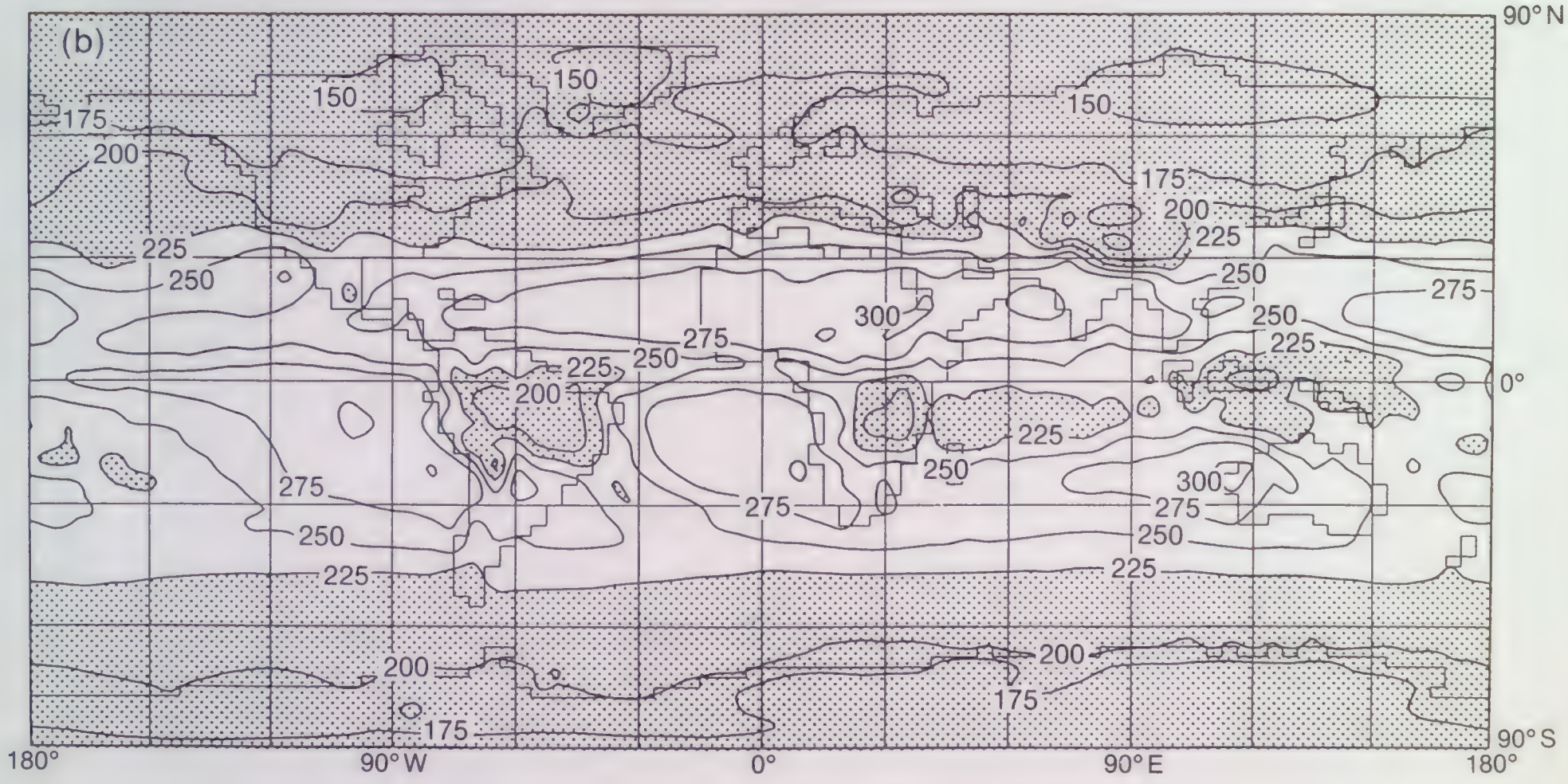

Figure 7(b)

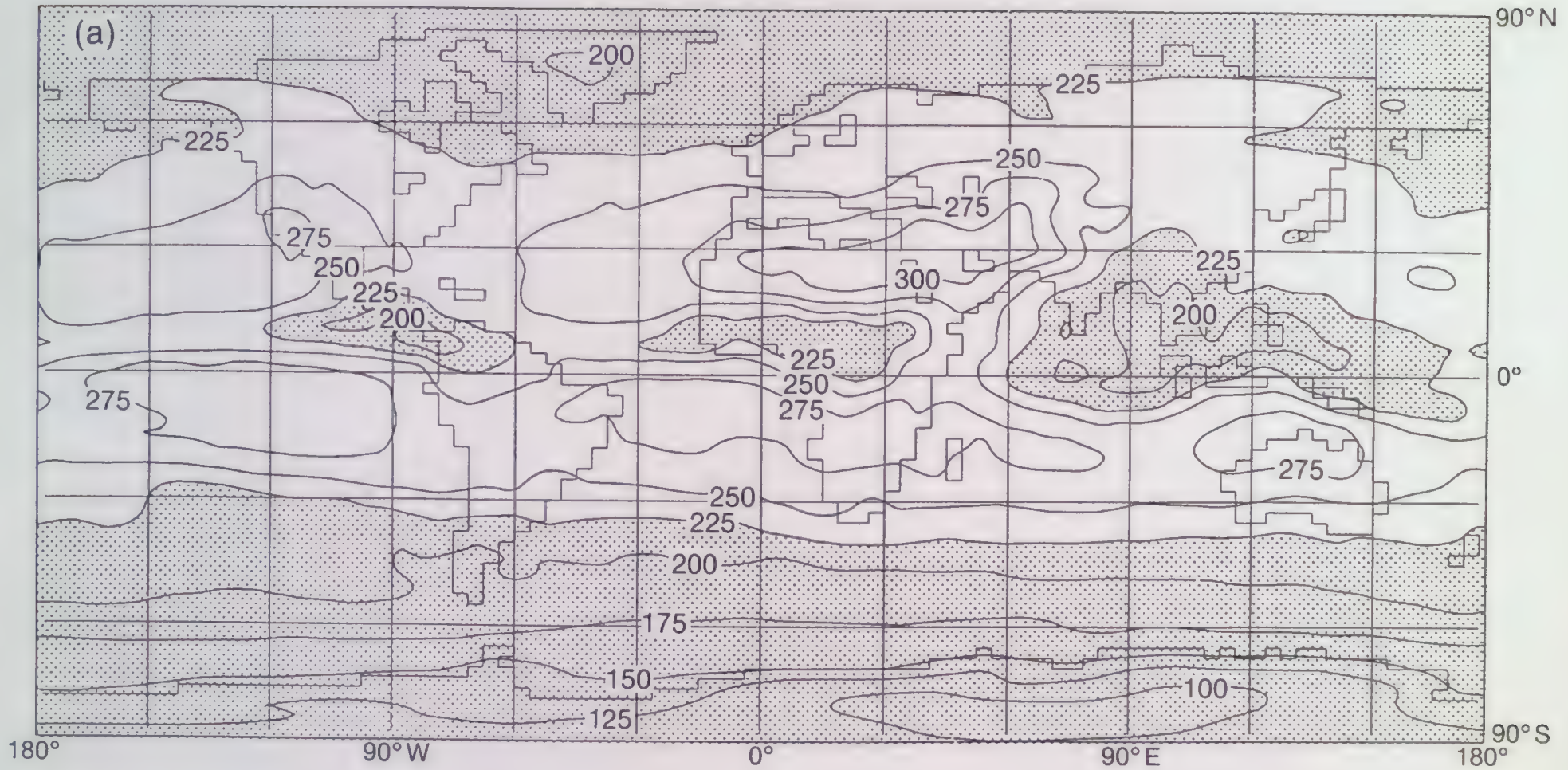

Figure 8(a)

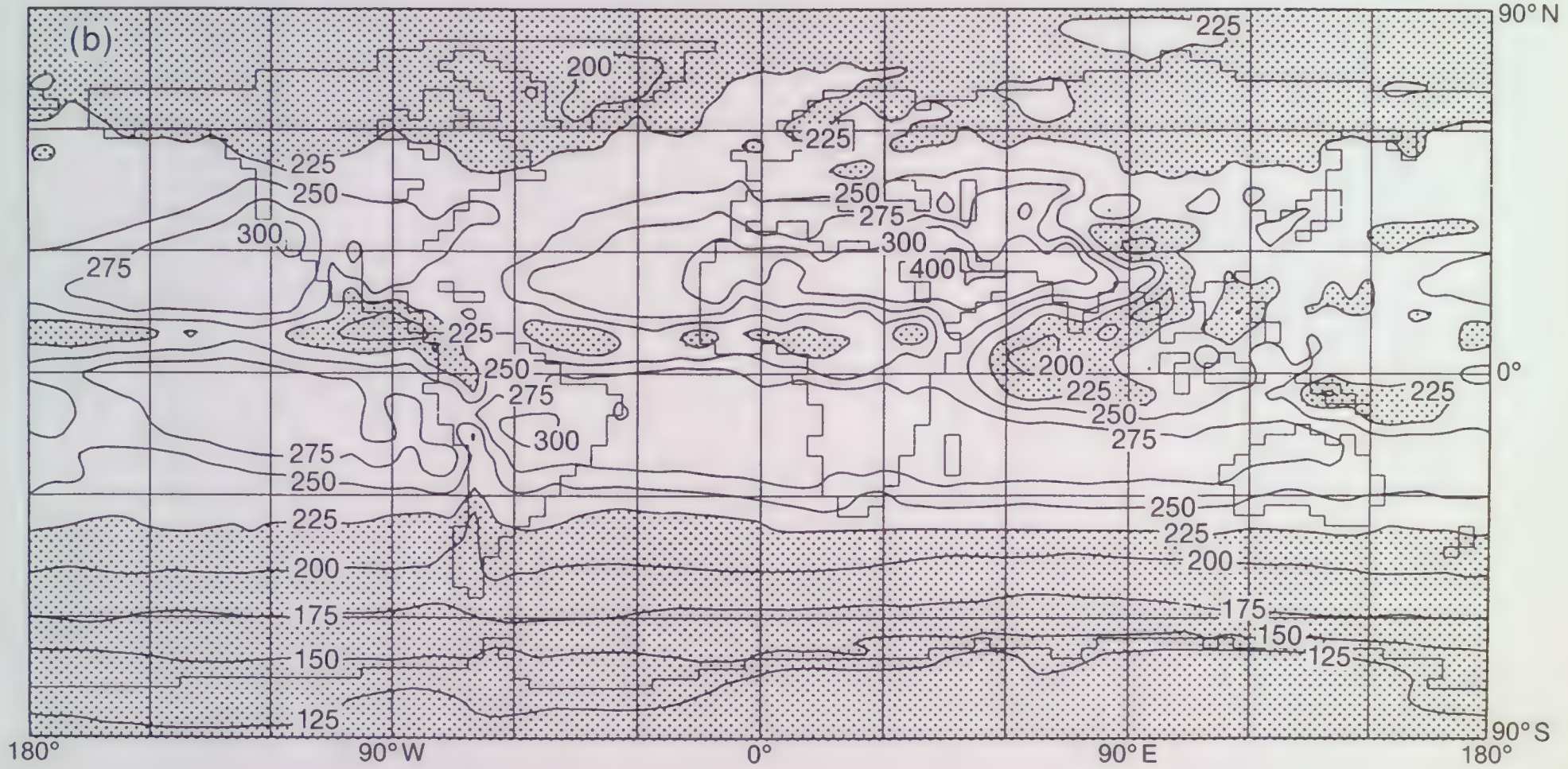

Figure 8(b)

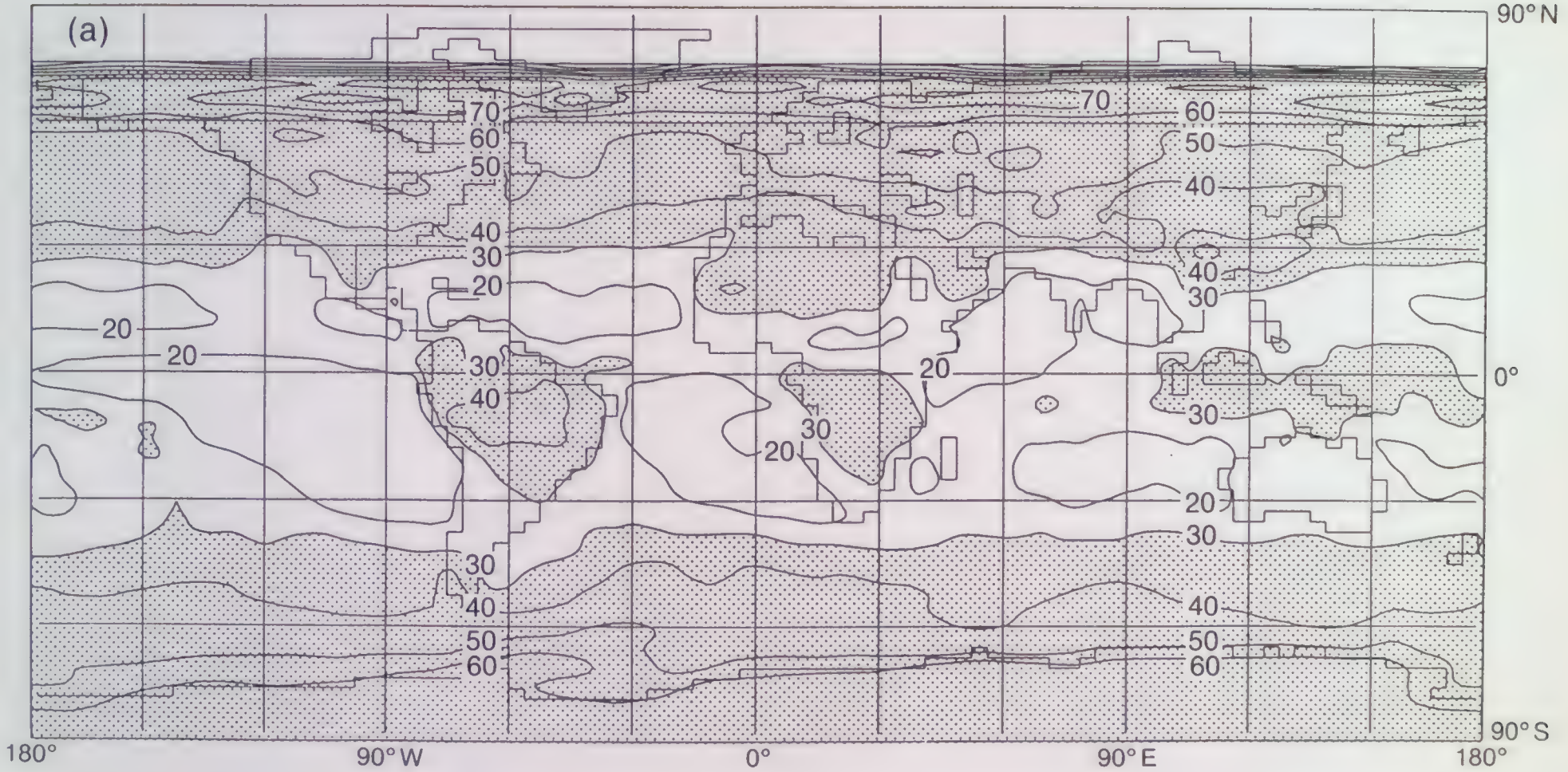
(a)
90° N
0°
90° S
180°
90° W
0°
90° E
180°
70
60
50
40
30
20
20
20
30
40
30
20
20
30
40
50
60
70
60
50
40
40
30
20
30
20
30
40
50
60

Figure 9(a)

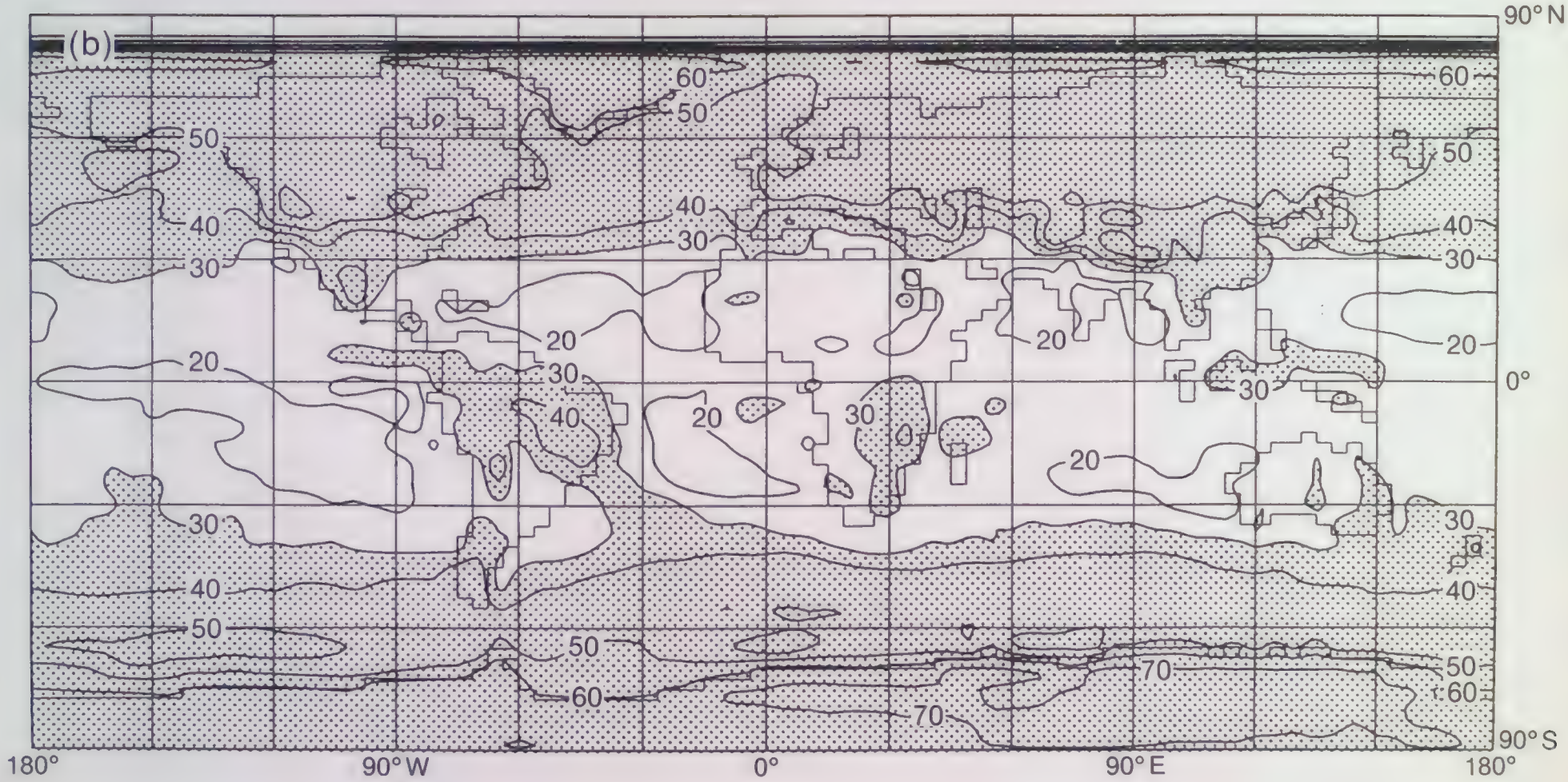

Figure 9(b)

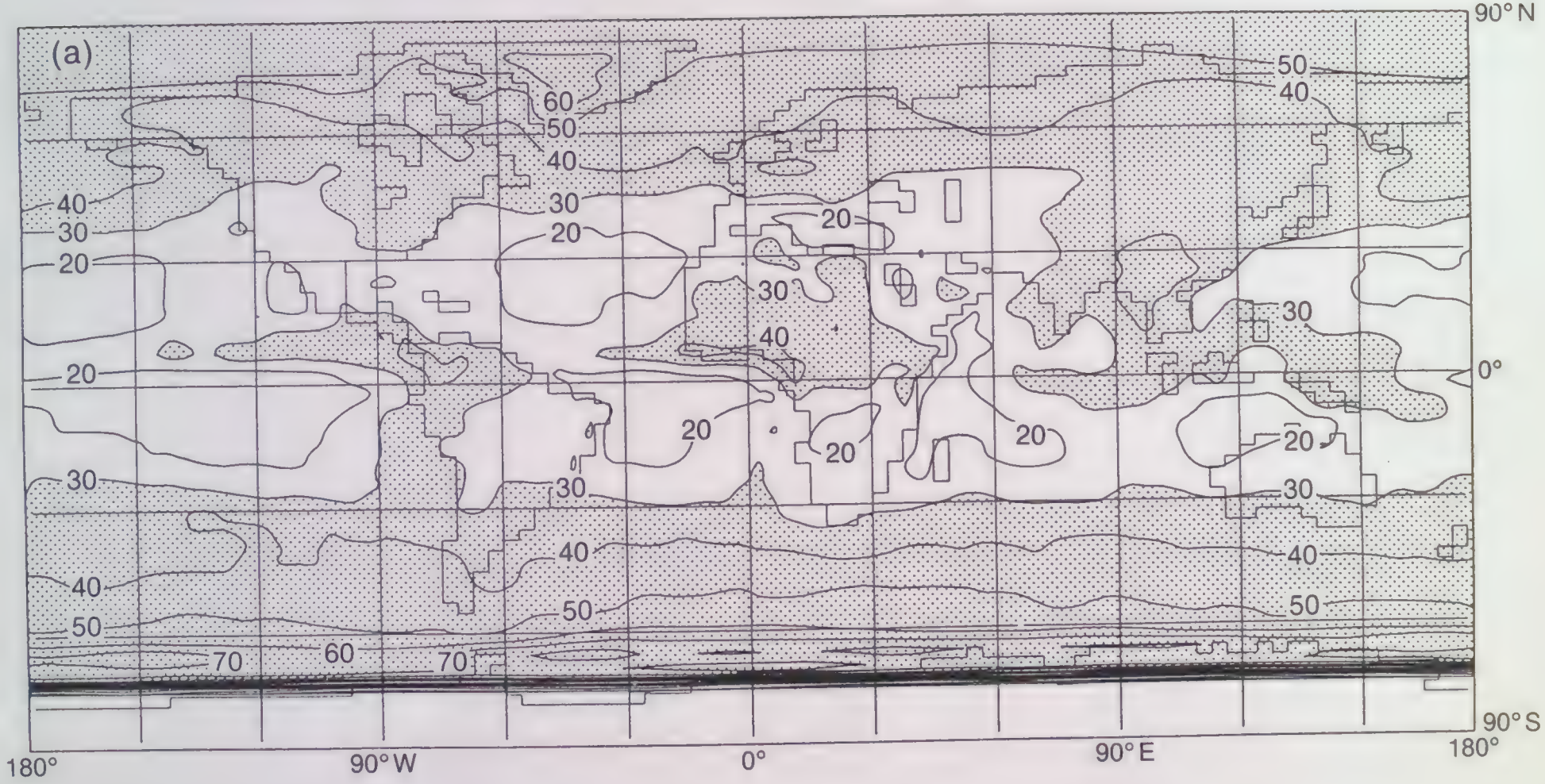

Figure 10(a)

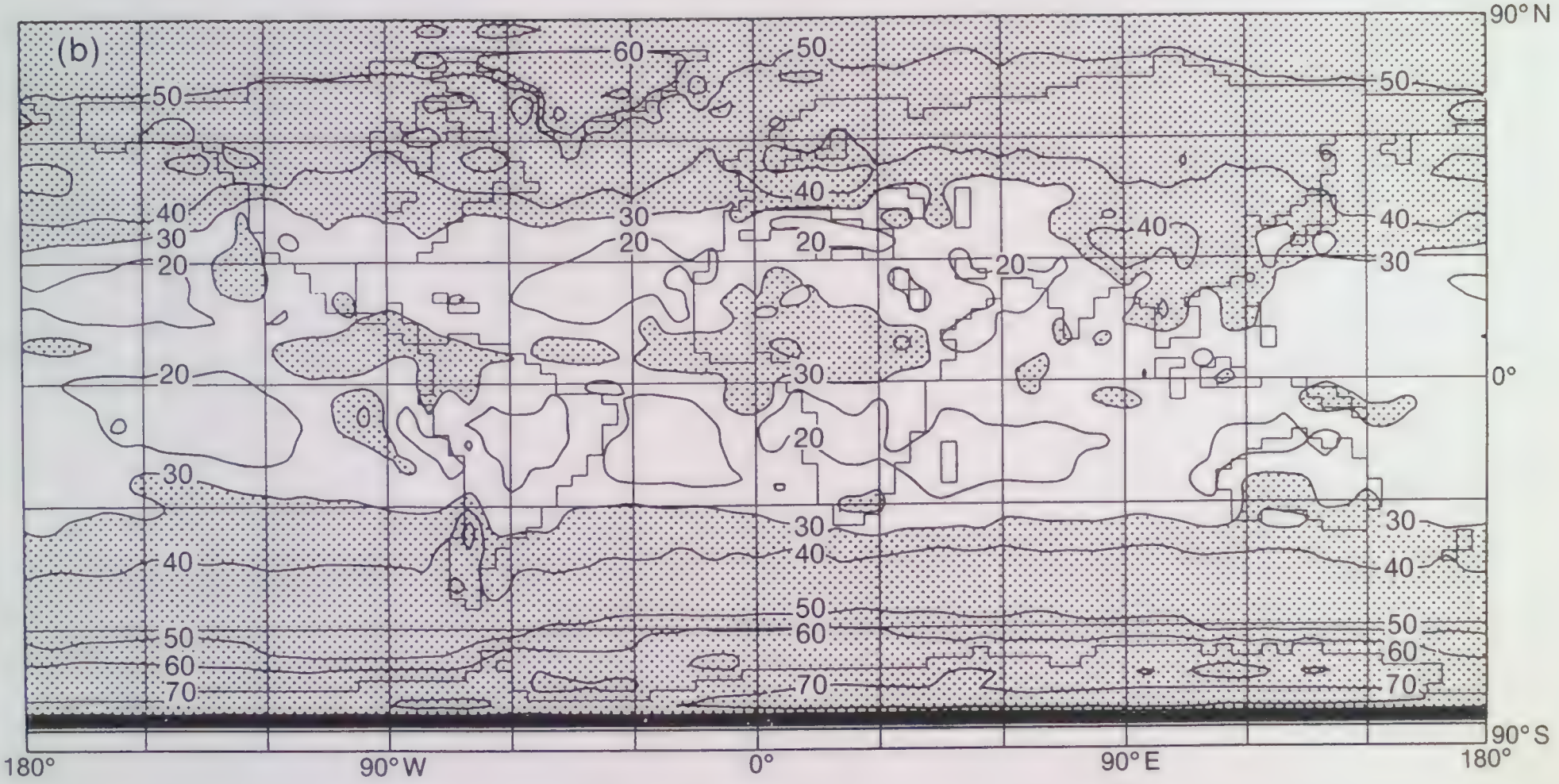

Figure 10(b)

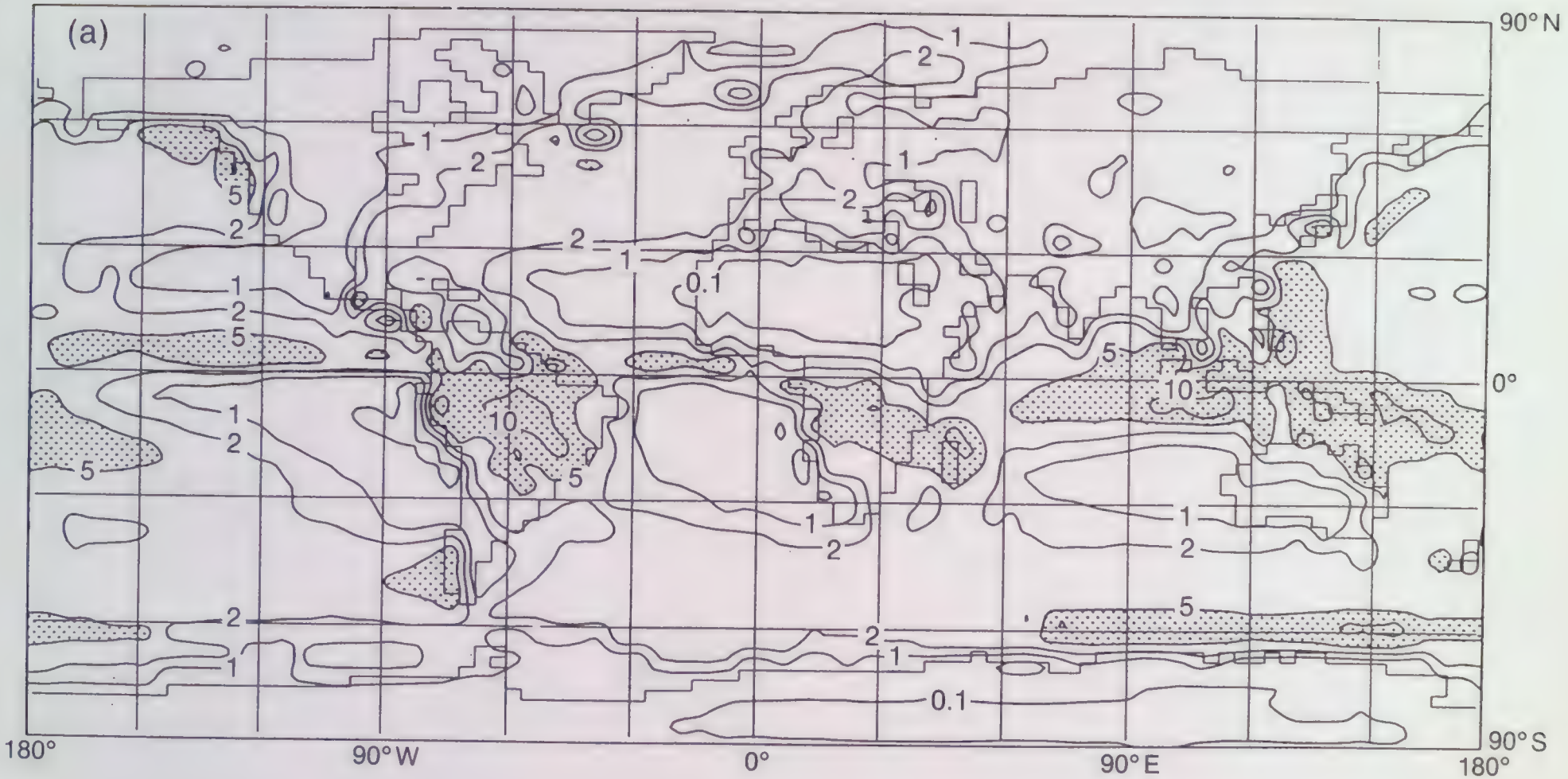

Figure 11(a)

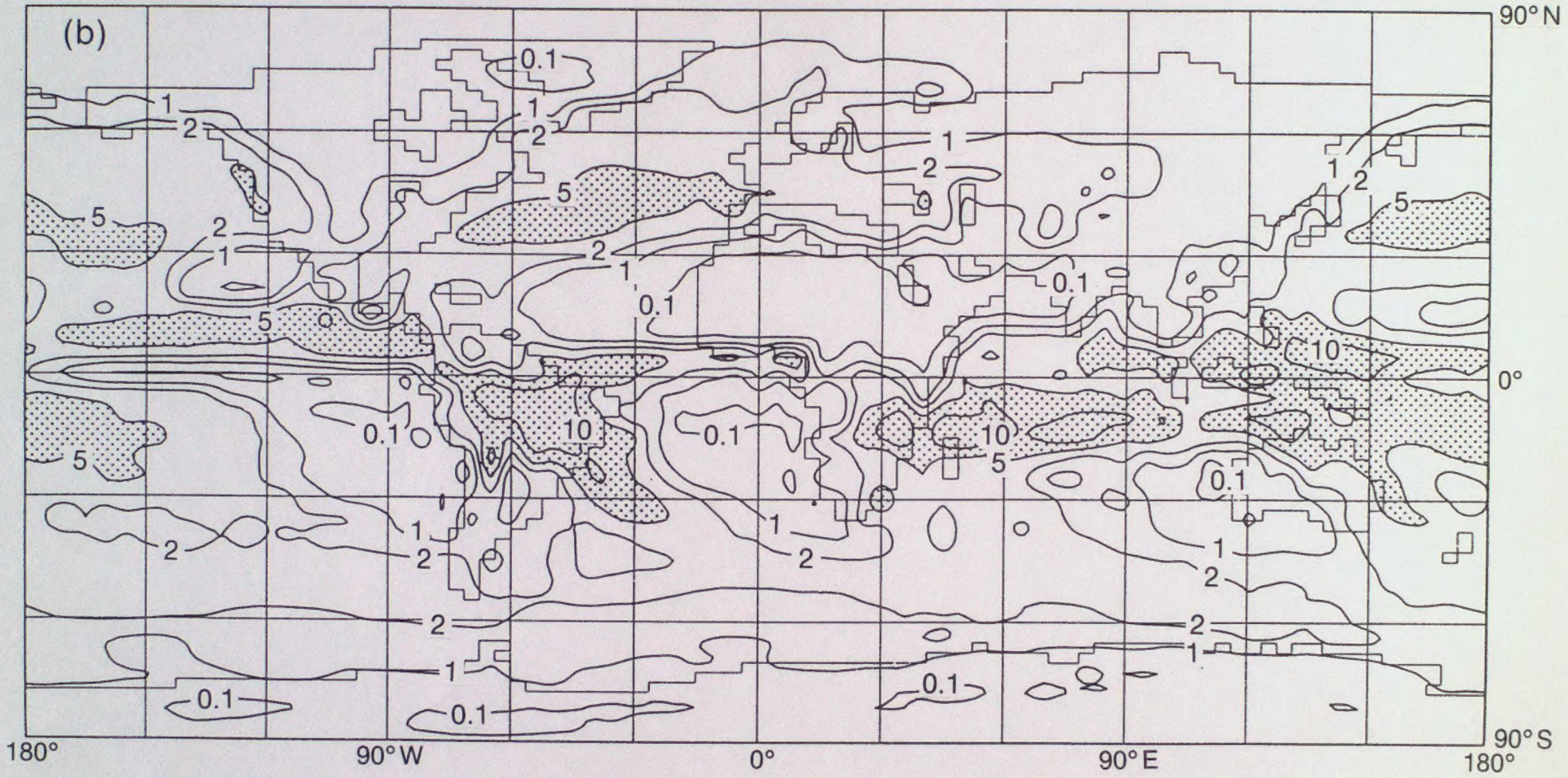

Figure 11 (b)

DYNAMICAL CLIMATOLOGY TECHNICAL NOTES

DCTN 1 June 1984
A scheme for incorporating the thermodynamic sea-ice model into a coupled ocean-atmosphere model.
C Gordon and M Bottomley

DCTN 2 Sept 1984
The parametrization of the upper ocean mixed layer in coupled ocean/atmosphere models.
C Gordon and M Bottomley

DCTN 3 Sept 1984
The response of a simple thermodynamic sea-ice model to GCM forcing appropriate for perennial sea-ice.
M Bottomley

DCTN 4 Sept 1984
Potential vorticity in the stratosphere derived using data from satellites.
S A Clough, N S Grahame and A O'Neill

DCTN 5 Sept 1984
Simulation of the seasonal cycle of SST using globally specified climatological data to force simple ocean models.
N S Grahame

DCTN 6 Sept 1984
Development of an improved GCM radiation scheme.
A Slingo and R C Wilderspin

DCTN 7 Sept 1984
On the specification of surface fluxes in coupled atmosphere/ocean general circulation models.
J F B Mitchell, C A Wilson and C M Price

DCTN 8 Sept 1984
A survey of possible repercussions of the Soviet river reversal programme on Arctic sea-ice.
M Cattle

DCTN 9 Oct 1984
A study of a strong stratospheric warming during January 1982
T D A Fairlie

DCTN 10 Nov 1984
An intercomparison of the Met O 11 M45 model and the Met O 20 11-level model on the Cyber 205
J F Dyson

DCTN 11 Nov 1984
Simulation of observed time series of temperature and precipitation over eastern England.
D M Reed

DCTN 12 Nov 1984
Forecasts and analyses of the onset of the Southwest monsoon.
R Kershaw

DCTN 13 Nov 1984
On modelling the effects of CO_2 on climate.
J F B Mitchell

DCTN 14 Dec 1984
Development of a revised longwave radiation scheme for an atmospheric general circulation model.
A Slingo and R C Wilderspin

DCTN 15 Jan 1985
Rossby wavetrains in the stratosphere forced by localised disturbances in the troposphere.
C J Marks (Oxford), A O'Neill and V D Pope

DYNAMICAL CLIMATOLOGY TECHNICAL NOTES

DCTN 16 Jan 1985
Observing system experiments using the Meteorological Office's 15-level model.
M A Bromley

DCTN 17 Feb 1985
Atmospheric general circulation simulation of the climate of the Mediterranean region.
M Cattle

DCTN 18 Feb 1985
Diurnal variation and cloud in a general circulation model.
C A Wilson and J F B Mitchell

DCTN 19 Feb 1985
The sensitivity of the Saharan region in a general circulation model.
W M Cunnington and P R Rowntree

DCTN 20 Mar 1985
The impact of aircraft observations on analyses and forecasts from the operational 15-level model.
B R Barwell

DCTN 21 Mar 1985
Non-linear effects on heat-induced circulation of the tropical atmosphere.
A E Gill and P J Phlips

DCTN 22 Apr 1985
Simulation of cloudiness with the U.K. Meteorological Office 11-layer AGCM.
A Slingo and R C Wilderspin

DCTN 23 Apr 1985
An integrated approach to the representation of cloud processes. R N B Smith

DCTN 24 May 1985
Nuclear Winter: Calculations of the shortwave radiative effects of soot aerosols.
A Slingo and P Goldsmith

DCTN 25 Jul 1985
Sea ice and the Antarctic winter circulation: a numerical experiment.
J F B Mitchell and T S Hills

DCTN 26 Jul 1985
A Budyko-Sellers model for study of ocean-atmosphere interaction.
W J Ingram

DCTN 27 Aug 1985
The effect of a shoaling thermocline on equatorially-trapped Kelvin waves.
A E Gill and B A King

DCTN 28 Sept 1985
CO_2 climate sensitivity and model dependence of results.
J F B Mitchell, C A Wilson and W M Cunnington

DCTN 29 Sept 1985
Handbook of the Meteorological Office 11-layer atmospheric general circulation model.
Volume 1 : Model Description
Edited by A Slingo

DCTN 30 Sept 1985
Impact of land surface variations on African rainfall in general circulation models.
P R Rowntree, M F Wilson and A B Sangster

DYNAMICAL CLIMATOLOGY TECHNICAL NOTES

DCTN 31 Nov 1985 The annual cycle of sea level in the eastern tropical Pacific.
G R Bigg and A E Gill

DCTN 32 Nov 1985 An analytic model of the heat-induced tropical circulation in the presence of a mean wind.
P J Philpe and A E Gill

DCTN 33 Nov 1985 The effect of resolution and diffusion on the simulated climate.
J F Dyson

DCTN 34 Jan 1986 Rossby adjustment over a step.
M K Davey, A E Gill, E R Johnson and P F Linden

DCTN 35 Jan 1986 Issues concerning the evaluation of effective surface roughness of heterogeneous terrain.
D J Carson

DCTN 36 Mar 1986 Climate sensitivity and past climates : evidence from numerical studies
J F B Mitchell

DCTN 37 Mar 1986 Parametrisations of land-surface processes in Meteorological Office numerical weather prediction and climate models
D J Carson

DCTN 38 Apr 1986 Modelling of land-surface processes and their influence on European Climate
D A Warrilow, A B Sangster and A Slingo

DCTN 39 Apr 1986 Simulation of climatic change due to increased CO_2
J F B Mitchell

DCTN 40 May 1986 On the interpretation of the Eliassen-Palm flux divergence.
Part I : Theory
D G Andrews

DCTN 41 June 1986 Experiments on tropical circulation with a simple moist model.
M K Davey and A E Gill

DCTN 42 Jun 1986 Parameter regimes for studying isolated eddies.
P D Killworth and M K Davey

DCTN 43 Jun 1986 A comparison of the impact of an envelope orography and of a parametrization of orographic gravity-wave drag on model simulations.
A Slingo and D W Pearson

DCTN 44 Jul 1986 The effect of a sea-surface temperature anomaly on a prediction of the onset of the south-west monsoon over India.
R Kershaw

DCTN 45 Jul 1986 An introduction to the parametrization of land-surface processes.
D J Carson

DYNAMICAL CLIMATOLOGY TECHNICAL NOTES

DCTN 46 Sept 1986 Lateral boundaries and the heat-induced flow in the tropical atmosphere.
P J Philpe and A E Gill

DCTN 47 Nov 1986 Simulation of the diurnal cycle of outgoing longwave radiation with an atmospheric GCM.
A Slingo, R C Wilderspin and S J Brentnall

DCTN 48 Feb 1987 A 2 x CO_2 climate sensitivity experiment with a global climate model including a simple ocean
C A Wilson and J F B Mitchell

DCTN 49 Feb 1987 Sensitivity of the Met O 20 11-layer model to increased land surface roughness length
C C Heasman

DCTN 50 Feb 1987 The influence of atmospheric waves on the general circulation of the middle atmosphere
D G Andrews

DCTN 51 Feb 1987 Transport mechanisms in the middle atmosphere: an introductory survey
D G Andrews

DCTN 52 Mar 1987 The Met O 20 stratosphere-mesosphere model
M Fisher

DCTN 53 Apr 1987 Simulations of linear and nonlinear disturbances in the stratosphere
A O'Neill and V D Pope

DCTN 54 Apr 1987 Aspects of dynamics of the middle atmosphere inferred using data from a satellite and from a numerical model
T D A Fairlie and A O'Neill

DCTN 55 Apr 1987 The seasonal evolution of the stratosphere in the northern hemisphere
A O'Neill and V D Pope

DCTN 56 Apr 1987 The adjustment of numerical weather prediction models to local perturbations
B R Barwell and R A Bromley

DCTN 57 Jun 1987 Climate simulations for 9000 years before present: Seasonal variations and the effect of the Laurentide ice sheet
J F B Mitchell, N S Grahame and K J Needham

DCTN 58 Aug 1987 Climatic effects of nuclear war: the role of atmospheric stability and ground heat fluxes.
J F B Mitchell and A Slingo

DCTN 59 Oct 1987 The stratospheric major warming of winter 1984/85: observations and dynamical inferences.
T D A Fairlie and A O'Neill

DCTN 60 Oct 1987 Some comparisons between the middle atmosphere dynamics of the southern and northern hemispheres
D G Andrews

DYNAMICAL CLIMATOLOGY TECHNICAL NOTES

DCTN 61	Jan 1988	Early winter in the northern stratosphere. M N Juckes and A O'Neill
DCTN 62	Feb 1988	Single column model tests of the Rowntree convection scheme using GATE data. D Gregory
DCTN 63	Mar 1988	The antarctic winter; simulations with climatological and reduced sea-ice extents. J F B Mitchell and C A Senior
DCTN 64	Mar 1988	An investigation of the Gates asynchronous coupling strategy using a simple energy-balance model. D L Roberts
DCTN 65	Apr 1988	The effect of improved physical parametrizations on simulations of cloudiness and the earth's radiation budget. A Slingo, R C Wilderspin and R N B Smith
DCTN 66	May 1988	Comparison of data and derived quantities for the middle atmosphere of the southern hemisphere. W L Grose and A O'Neill
DCTN 67	Aug 1988	Progress and future developments in modelling the climate system with general circulation models. P R Rowntree
DCTN 68	Aug 1988	A scheme for predicting layer clouds and their water content in a general circulation model. R N B Smith